Journal of Medicinal Chemistry

ARTICLE

pubs.acs.org/jmc

Design, Synthesis, and Functionalization of Dimeric Peptides Targeting Chemokine Receptor CXCR4

Oliver Demmer,[†] Ingrid Dijkgraaf,[‡] Udo Schumacher,[§] Luciana Marinelli,[∥] Sandro Cosconati,[∥] Eleni Gourni,[‡] Hans-Jürgen Wester,[‡] and Horst Kessler[†,⊥,*]

[†]Institute for Advanced Study and Center of Integrated Protein Science at the Department Chemie, Technische Universität München, Lichtenbergstrasse 4, D-85748 Garching, Germany

[‡]Lehrstuhl für Pharmazeutische Radiochemie, Technische Universität München, Walther-Meissner-Strasse 3, 85748 Garching, Germany

[§]Institute for Anatomy II: Experimental Morphology, Universitätsklinikum Hamburg-Eppendorf, Martinistrasse 52, 20246 Hamburg, Germany

[∥]Dipartimento di Chimica Farmaceutica e Tossicologica, Università di Napoli "Federico II", Via D. Montesano, 49-80131 Napoli, Italy

[⊥]Chemistry Department, Faculty of Science, King Abdulaziz University, P.O. Box 80203, Jeddah 21589, Saudi Arabia

Supporting Information

ABSTRACT: The chemokine receptor CXCR4 is a critical regulator of inflammation and immune surveillance, and it is specifically implicated in cancer metastasis and HIV-1 infection. On the basis of the observation that several of the known antagonists remarkably share a C_2 symmetry element, we constructed symmetric dimers with excellent antagonistic activity using a derivative of a cyclic pentapeptide as monomer. To optimize the binding affinity, we investigated the influence of the distance between the monomers and the pharmacophoric sites in the synthesized constructs. The affinity studies in combination with docking computations support a two-site binding model. In a final step, 1,4,7,10-tetraazacyclododecane-1,4,7,10-tetraacetic acid (DOTA) was introduced as chelator for (radio-)metals, thus allowing to exploit these compounds as a new group of CXCR4-binding peptidic probes for molecular imaging and endoradiotherapeutic purposes. Both the DOTA conjugates and some of their corresponding metal complexes retain good CXCR4 affinity, and one ^{68}Ga labeled compound was studied as PET tracer.

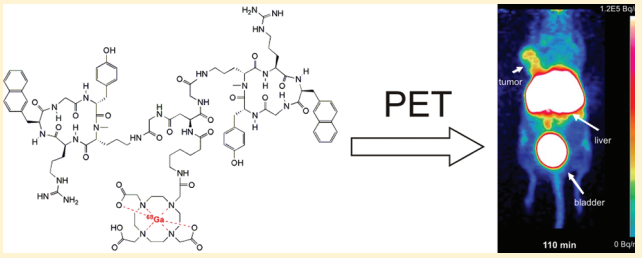

INTRODUCTION

CXCR4 is one of the most prominent members of the chemokine receptor family and a central component of the communication pathways in the body. This seven-transmembrane G-protein coupled receptor (GPCR) and its natural ligand, the stromal cell-derived factor (CXCL12; formerly known as SDF1) are part of a signaling system involved in cell migration of organogenesis, hematopoiesis, inflammation, and immune response.[1] Because of this central role, the CXCR4−CXCL12 interaction is involved in various severe diseases like cancer, HIV, and autoimmune diseases that are seemingly independent at first glance. The therapeutic potential of CXCR4 antagonists has already been shown for the treatment of HIV infection, cancer, and rheumatoid arthritis.[2−5] Other potential therapeutic uses of CXCR4 antagonists have been described for asthma, the mobilization of stem cells for stem cell transplantations, and the attenuation of pain, and they are also discussed for the treatment of neurological diseases.[6] Our focus is to find an approach for personalized medicine for cancer by providing tools for diagnosis and treatment. CXCR4 is involved in three fundamental stages of various cancer types (e.g., in lung, breast, prostate, ovarian, colon, melanoma, brain cancers): primary tumor growth, migration of cancer cells, and establishment of metastases. In result CXCR4 is overexpressed in more than 70% of cancers, generating the need for personalized treatment through a combination of diagnosis and treatment.

As part of our ongoing effort to develop high affinity CXCR4 binding ligands for molecular imaging and endoradiotherapeutic purposes, we were interested in introducing DOTA, a chelator often used for a wide variety of medically interesting metal ions.[7] Because functionalization of a given ligand is often accompanied by a significant reduction in binding affinity, we explored again the concept of dimerization (multimerization) to compensate for potential impairment of binding affinity.[8−11]

The concept of polyvalency, and herein more specifically dimers, is particularly interesting in the case of CXCR4 due to the peculiar structure of the receptor which was first hypothesized to contain two neighboring binding sites, one responsible for the affinity and the other for signaling function.[12]

Received: July 20, 2011
Published: September 12, 2011

dx.doi.org/10.1021/jm2009716 | J. Med. Chem. 2011, 54, 7648–7662

Scheme 1. Dimeric CXCR4 Antagonists 1−3

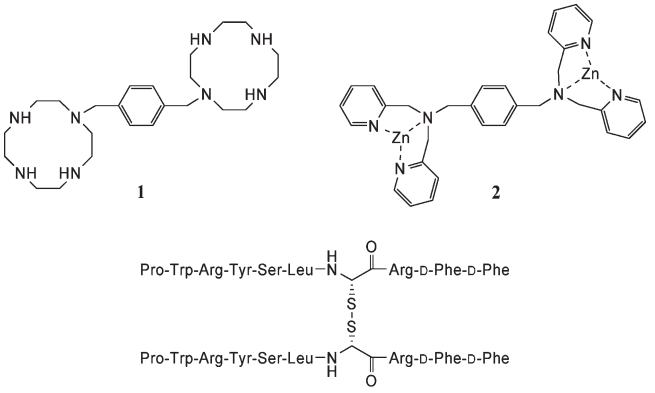

Scheme 2. the Original Cyclic Pentapeptide FC131 4 and Our Derivative 7 Used for Dimerization

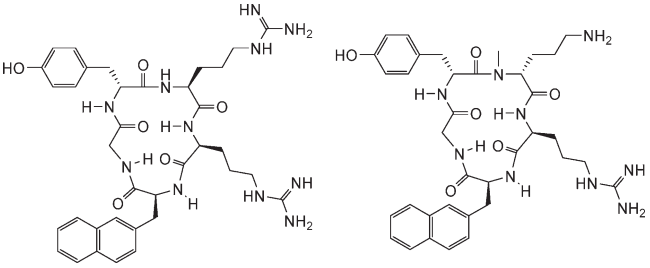

On the other hand, several known CXCR4 antagonists like the FDA approved drug Mozobil (AMD3100 **1**; Scheme 1) contain a C_2 symmetry element,[13] and its success story has sparked the development of further excellent ligands.[14] Not only **1** and its derivatives exhibit this C_2 symmetry element but also other small molecules (e.g., dipicolylamine-zinc(II) compounds; **2**) as well as peptidic dimers (e.g., S1D **3**) that have been found independently (Scheme 1).[15,16] Although the structure and thus its exact symmetry has not been fully revealed, the orphan drug CTCE-9908 is also a dimeric peptidic CXCR4 antagonist.[5,17] While many of the above-cited ligands would well fit in the "two-site model" of the receptor, it is well-known that CXCR4 can form homo- and heterodimers, and this has to be considered as an alternative explanation why some symmetric dimers have superior binding properties in comparison to their monomers.[18] However, the spacing of the ligand-binding sites in the crystal structure of dimeric β2-adrenergic receptor matches the ∼40 Å distance, and this was recently demonstrated to be approximately the same in the CXCR4 dimers,[19] thus suggesting that the formation of a functional 2:2 SDF-1:CXCR4 complex might be plausible, while for smaller ligands the same is unimaginable and the "two-site model" of the receptor seems to be the most reliable hypothesis.

However, the functional importance of dimerization remains incompletely characterized, although a considerable body of data suggests that it has important in vivo pharmacological effects. Besides these CXCR4-specific considerations for the construction of dimeric ligands, dimers and higher multimers have been used in other fields of medicinal chemistry.[10,11,20,21] Especially in molecular imaging, we and others could demonstrate the power of the multivalency approach to improve target/ligand interaction and thus imaging contrast.[8,22]

As a starting point for our ligand development, we have chosen **4** (FC131, Scheme 2), which was developed by Fujii et al. by downsizing of polyphemusin II.[23−25] It combines high CXCR4 affinity with the commonly low toxicity of peptides and a high stability toward enzymatic degradation associated with cyclic pentapeptides.[25,26] Additionally, this class of ligands are believed to have less side effects when used as pharmaceuticals as they are inverse agonists, especially in comparison with **1**, which is a partial agonist.[4,27] In a very recent study, it could be shown that using very long spacers with length approximately from 20 to 80 Å can have positive effects on binding affinity.[28] In this study, evidence was provided that two CXCR4 receptors can be addressed by two ligands in one large molecule when they are separated by a long spacer. In contrast, our studies of ligand oriented design focus on dimers connected by shorter spacers to mimic known ligands. Here two (different) binding sites in the same monomer can be addressed (see below).

After further modifications of **4**, including an *N*-methylation for affinity enhancement and the elucidation of a side chain suitable for additional modifications, we selected *cyclo*(D-Tyr[1]-D-[*N*Me]Orn[2]-Arg[3]-Nal[4]-Gly[5]) (D-[*N*Me]Orn = N^{α}-methyl-D-ornithine; Nal = L-3-(2-naphthyl)alanine) **7** for our dimerization studies.[29,30] Because the side chain of D-[*N*Me]Orn[2] is the "least important residue" in this peptide and is quite amenable to acylation, we used D-[*N*Me]Orn[2] as anchor point for dimerization.[31]

Herein we describe the synthesis of dimers and evaluation of the optimal distance between the monomeric units. Subsequent comparison of the affinity improvement with other C_2 symmetric CXCR4 ligands in combination with the exchange of supposedly important pharmacophoric residues gives hints on a different binding mode originating from the design of **4**. Finally DOTA is introduced to the dimers as chelator allowing preparation of (radio-)metal ion complexes of peptides with promising potential for therapeutic and diagnostic applications. The recent advent of the first and unique X-ray structures of CXCR4 receptor alone and in complex with the antagonist small molecule IT1t and the cyclic peptide CVX15 give us the opportunity to model the interaction of the cyclic peptide monomer **7** and the dimeric peptide **10** with the receptor.[19]

RESULTS

Synthesis. Monomeric, *N*-methylated cyclic pentapeptides were synthesized according to established procedures.[32] Glycine was attached to the resin to avoid racemization during the cyclization step and to allow for easier cyclization due to turn preformation caused by the N-terminal D-amino acid.[33] The peptide chain was elongated until ornithine with standard Fmoc solid phase peptide synthesis (SPPS). N^{α}-2-Nitrobenzenesulfonyl (nosyl; Ns) protected N^{δ}-Boc-D-ornithine was synthesized as building block because the Ns group activates the N^{α} for fast on-resin *N*-methylation.[32,34] N^{α}-Alloc-N^{δ}-Fmoc-D-ornithine was used in branched peptides **6**, **8**, and **9** to modify the side chain. Alloc was cleaved after acylation of the side chain and the N^{α}

dx.doi.org/10.1021/jm2009716 |J. Med. Chem. 2011, 54, 7648–7662

Scheme 3. Synthesis of the N^{α}-Methylated, Branched, Cyclic Pentapeptides[a]

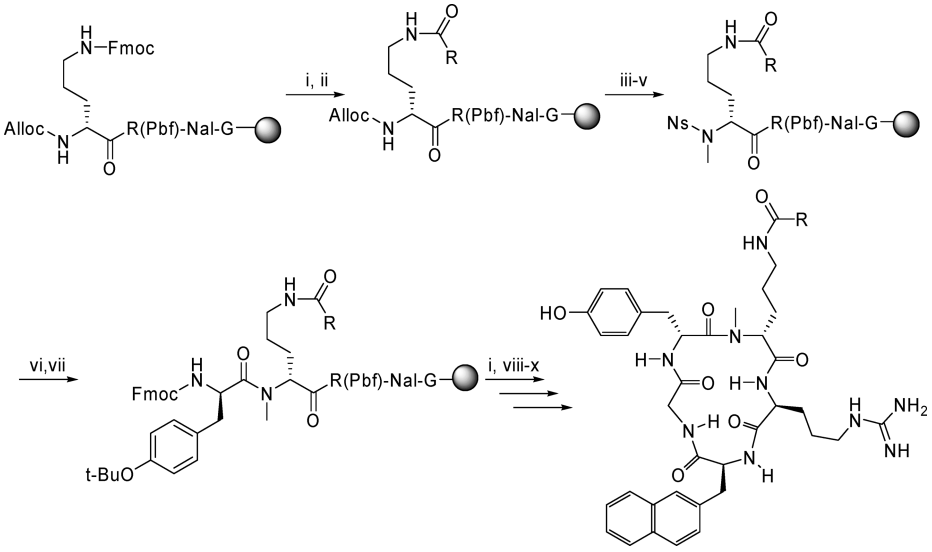

[a] Reagents: (i) 20% piperidine, NMP; (ii) Fmoc-AA, TBTU, HOBT, DIEA, NMP; (iii) $Pd(PPh_3)_4$, $PhSiH_3$, DCM; (iv) NsCl, collidine, NMP; (v) MeOH, DIAD, PPh_3, THF; (vi) DBU, 2-mercaptoethanol, NMP; (vii) Fmoc-AA, HATU, HOAt, DIEA, NMP; (viii) 20% HFIP, DCM; (ix) DPPA, $NaHCO_3$, DMF; (x) 95% TFA, 2.5% TIPS, 2.5% H_2O.

Scheme 4. Construction of Diacidic Building Blocks Shown Exemplary for the Homo-Bβ-Aspartic Acid Linker

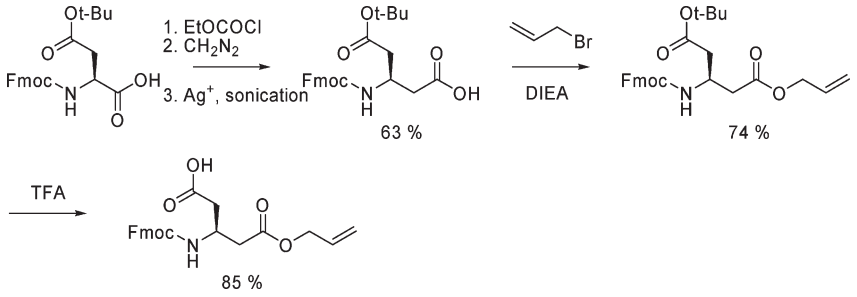

reprotected with Ns and then *N*-methylated (Scheme 3). After cleavage of the Ns group, D-tyrosine was attached using HATU and subsequently the linear peptide was cyclized and deprotected to yield the pure peptide after HPLC separation.

Peptide monomers were dimerized by coupling in DMF solution, with DIEA and 0.5 equiv of the corresponding diacid. The distance between the monomers was varied by using linear diacids with 3−16 carbon atoms. In contrast to this procedure, dimer **11** with one active and one inactive monomer was built by coupling the inactive monomer with a 10-fold excess of glutaric acid to suppress dimerization. After HPLC purification, the active monomer was attached in a second step in equimolar amounts.

To allow the introduction of functional moieties into the dimeric peptides, trifunctional linkers were used. Two diacid building blocks were synthesized to vary the distance between the two peptidic units that contain an additional amine for the introduction of further spacing and DOTA units. They were constructed on solid support containing tris(*t*-Bu)DOTA connected via an 6-aminohexanoyl unit to aspartic acid or homobeta-aspartic acid, respectively. The symmetric homobeta-aspartic acid unit was built from the standard L-aspartic acid used for SPPS containing Fmoc and *t*-Bu protection by introducing the methylene group via the Arndt−Eistert homologization.[35] The protected aspartic acid was reacted with diazomethane, and the silver-catalyzed Wolff rearrangement gave the homobeta-amino acid (Scheme 4). For both aspartic acids, the second acid group was protected with allylbromide so that this allyl group can be cleaved orthogonally to the *t*-Bu groups of tris(*t*-Bu)DOTA. The free DOTA moiety was then obtained in the final acidic deprotection step with HCl. The peptidic linkers were constructed by attaching the aspartic acid building blocks to the resin followed by standard SPPS to attach 6-aminohexanoic acid and tris(*t*-Bu)DOTA and Pd-catalyzed allyl deprotection before the linker was cleaved from the resin and purified by HPLC (see Supporting Information).

The monomeric peptide units were coupled with the DOTA labeled linkers described above, deprotected, and if required also transformed into the corresponding In^{3+} chelate in an one-pot reaction (see Supporting Information).

Biological Results. Compound **5** was resynthesized and tested to ensure the comparability of our testing system with the one used in literature (Table 1).[29] The inactive monomer **6** was generated by exchanging the crucial arginine residue isosterically with the uncharged citrulline. It also carries the

Table 1. Monomeric and Dimeric CXCR4 Ligands and IC_{50} Values[a]

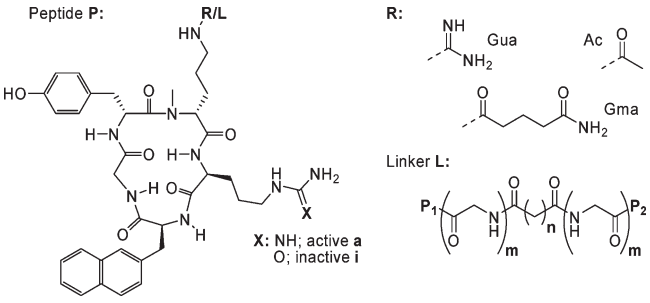

		L		
compd	R	*m*	*n*	IC_{50} [nM]
5	Gua			2 ± 2
6[b]	Ac			1000
7	H			6 ± 1
8	Ac			60 ± 20
9	Gma			67 ± 5
10		0	3	4 ± 2
11[c]		0	3	19 ± 7
12		0	2	12 ± 8
13		0	4	4 ± 1
14		0	6	3 ± 1
15		0	8	2 ± 1
16		0	11	4 ± 7
17		0	14	33 ± 17
18		1	1	8 ± 5
19		1	2	6 ± 2
20		1	3	14 ± 2

[a] Mean value of at least two 2 experiments. [b] inactive monomer (i). [c] mixed dimer with one active (a) and one inactive monomer (i).

acetylated ornithine moiety to stay as close as possible to the acylated motif present in the dimers. In **7**, the less important arginine was exchanged by ornithine to conserve the number of carbon atoms in the side chain and simultaneously generate an amine that allows acylation and dimerization having an IC_{50} of 6 nM. Modification of the ornithine side chain by acylation impairs the binding affinity so that **8** and **9** are more than 10-fold less active than **7**.

The dimers **10**−**20** were used to elucidate the optimal spacer lengths, with **11** being an exception as it contains one active and one inactive peptide unit which was used to investigate the binding mode. The optimal distance of the dimers is not well-defined, with a broad range of 5−10 carbon atoms in the spacer and an affinity of 2−4 nM. **15** has the best binding affinity with 2 nM, which is more than 30 times more active than the acetylated monomer **8** and had 3-fold higher activity than the monomer **7** from which it was synthesized. The mixed dimer **11** has an IC_{50} of about 20 nM, which is almost in the middle of the affinity range between the less affine monomers **8** and **9** and the better dimers with two active peptide moieties. The dimers with an additional glycine spacing unit **18**−**20** do not reach the activity level of the most active dimers but are still 10 times more affine than the acylated monomers.

The dimers additionally containing the DOTA moiety **21**−**28** have a wide range of affinities ranging from nearly 10 nM to almost 100 nM (Table 2) depending on the spacer and the chelation with indium. With the exception of the dimers **23** and **24**, the indium chelates show a higher CXCR4 affinity than their free DOTA counterparts. The most active compounds, **25**−**28**, contain an additional glycine spacer which corresponds in combination with the DOTA conjugated spacer to the length found in the best dimer **15**.

25 was labeled with ^{68}Ga, and the labeled tracer was used for initial in vivo evaluation in OH1 h-SCLC tumor bearing nude mice. Biodistibution studies carried out 60 min after the intravenously injection of the labeled compound into the tail vain of mice (Table 3). Attention being focused on the experimental tumor and on CXCR4 bearing organs, such as spleen and liver, because it is known that high CXCR4 mRNA expression is observed. At 60 min pi, the liver was the organ with the highest accumulation of radioactivity (44.3 ± 5.5%ID/g).[36] Relatively high accumulation was also observed in lung (2.1 ± 0.3%ID/g), spleen (4.0 ± 0.6%ID/g), and kidney (3.3 ± 0.5%ID/g). The accumulation of the radioactivity in the tumor (2.1 ± 0.5%ID/g) was higher than in the blood (1.9 ± 0.3%ID/g) and the muscle (0.4 ± 0.1%ID/g). Co-injection of a ^{nat}Ga containing CXCR4 specific PET tracer (compound **2c** ref 31) resulted in lower tumor uptake with a reduction of approximately 50%, demonstrating retention of ^{68}Ga-**25** in the experimental tumor by CXCR4-binding. The increased kidney uptake under blocking conditions also confirms competition of tracer binding to CXCR4 receptors by the cold peptide. On the basis of the suboptimal biodistribution, specificity of binding of the new tracer to CXCR4 receptors was demonstrated in a competition study by coinjection of an excess of cold receptor ligand in one mouse. In such cases, i.e. when the biodistribution of a tracer is found to be suboptimal, we suggest demonstrating further in vivo data, such as metabolic stability or specificity of binding, only on a very small number or cohort of animals and to refrain from aiming to quantify further in vivo values with limited or no further scientific impact with high accuracy. Although only one animal has been used, a quantitative blockade is always a clear indicator for high specificity of binding. As a consequence of reducing the uptake in the tumor by blockade, the majority of the tracer is now directed and retained in organs known to typically retain (basic) peptides, such as somatostatins, i.e. the kidneys and the spleen.

In parallel with biodistribution studies, PET imaging of ^{68}Ga-**25** was performed to visualize the uptake in the various organs. The PET images were in accordance with the data from the ex vivo biodistibution. As revealed by organ analyses, high accumulation of ^{68}Ga-**25** was obtained in the liver, however, still allowing visualization of the tumor.

DISCUSSION

To compare the effect of dimerization, compounds **8** and **9** were synthesized having an acylated amine at the ornithine N^{δ} of the monomer. Compound **8** is less affine by a factor of 10 in comparison to **7**, with the free amine showing that the basic group at this position has positive effects, even so, it is the most unimportant side chain. To be able to exclude effects of the spacing unit toward binding affinity, compound **9** was synthesized carrying a glutaric amide at the ornithine side chain. This compound shows even less affinity toward CXCR4 than the

dx.doi.org/10.1021/jm2009716 |J. Med. Chem. 2011, 54, 7648–7662

Table 2. Dimeric DOTA Labeled Peptides and Their IC_{50} Values[a]

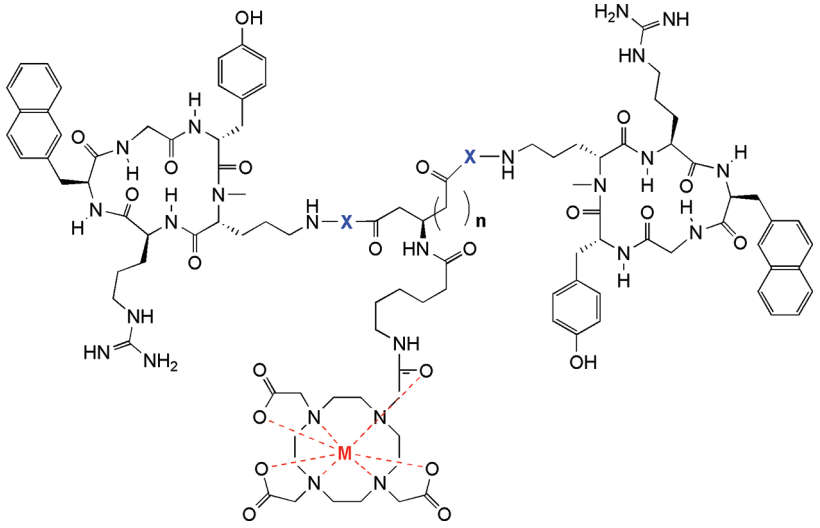

compd	X	*n*	M	IC_{50} [nM]
21		0		98 ± 13
22		0	In^{3+}	76 ± 22
23		1		31 ± 14
24		1	In^{3+}	81 ± 8
25	Gly	0		39 ± 2
26	Gly	0	In^{3+}	15 ± 3
27	Gly	1		17 ± 7
28	Gly	1	In^{3+}	13 ± 5

[a] Mean value of at least 3 experiments.

acetylated peptide, demonstrating that the spacer itself does not contribute beneficially to binding affinity (Table 1).

In comparison with the acetylated monomer **8**, all dimers, connected by a diacid with less than 16 carbon atoms, show an enhanced affinity (Table 1). Dimer **10** spaced by glutaric acid has a more than 10-fold higher affinity than monomer **9** with just glutaramide attached, showing that not the spacer but the second peptide unit is responsible for enhanced affinity. The optimal distance between the two peptides has a broad spacer range of 5−10 carbon atoms with an IC_{50} of 2−4 nM and no distinct minimum, suggesting some flexibility of the dimers. However, when the distance is further increased to 13 or 16 atoms, the affinity becomes lower.

We further investigated if two identical binding pockets are addressed by the dimers by exchanging an important pharmacophoric group of the monomer. Arg^3 of **8** was substituted by L-citrulline (Cit), which leads to a complete loss of affinity of the monomer **6**. However, the combination of one active with one inactive cyclopentapeptide gives the asymmetric dimer **11**, which is less affine than the corresponding symmetric dimer **10** but exhibits more than three times better affinity than compound **9**, which carries the same spacing group but without a second peptide unit. Hence, the guanidine group of the second peptide is beneficial for binding affinity but not as essential as in the first binding pocket. This in turn shows that both binding pockets are not identical, as the second one can also bind cyclic pentapeptides but does not require the same

Table 3. Biodistribution of ^{68}Ga-25 in OH1 Bearing-Tumor Nude Mice 60 min pi[a,b]

organ	unblocked[a] (*n* = 5)	blocked[a,b] (*n* = 1)
blood	1.87 ± 0.29	2.1
heart	1.14 ± 0.19	2.5
lung	2.11 ± 0.27	11.0
liver	44.31 ± 5.56	43.0
pancreas	0.81 ± 0.29	1.4
spleen	3.98 ± 0.60	15.6
kidney	3.26 ± 0.51	34.8
adrenal glands	1.48 ± 0.20	2.6
stomach	1.04 ± 0.39	4.1
intestine	1.30 ± 0.42	3.0
muscle	0.37 ± 0.07	1.0
OH1 tumor	2.08 ± 0.48	1.1
tumor/heart	1.81 ± 0.22	0.5
tumor/liver	0.05 ± 0.01	0.02
tumor/kidney	0.63 ± 0.09	0.03
tumor/muscle	5.96 ± 2,36	0.5

[a] Data are expressed as % ID/g tissue ± SD. [b] Blocking was achieved by coinjection of 100 μg/mouse of a ^{nat}Ga-tracer (compound **2c** in ref 31).

dx.doi.org/10.1021/jm2009716 |J. Med. Chem. 2011, 54, 7648–7662

Scheme 5. Schematic Comparison of Polyphemusin II (Upper Part) and a Dimeric Ligand (Lower Part)[a]

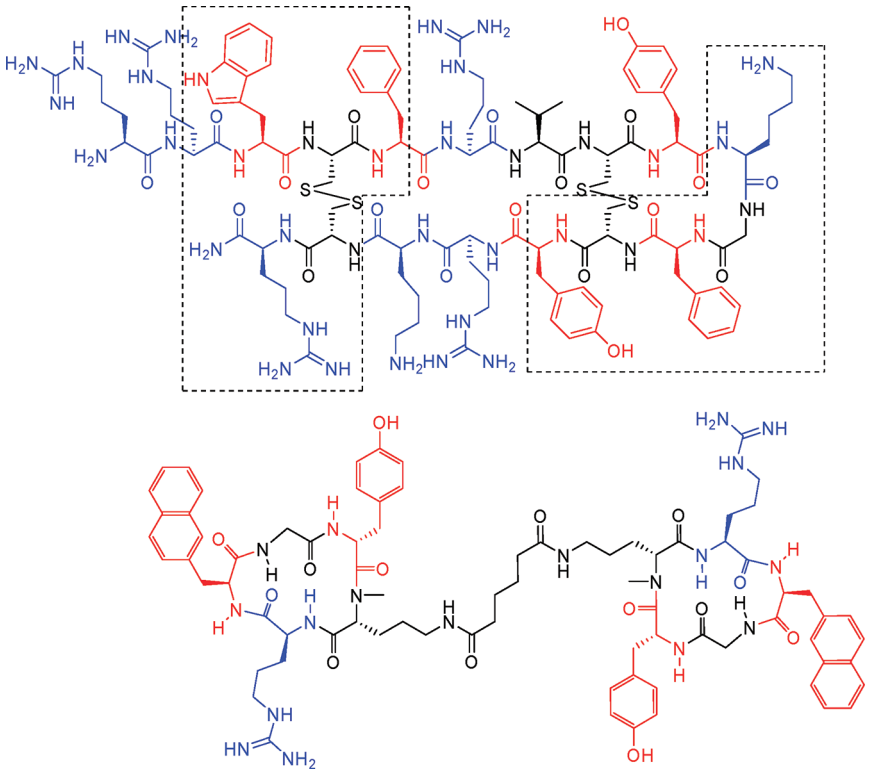

[a] Aromatic amino acids are highlighted in red and basic in blue. The boxed regions of polyphemusin II are assumed to correspond to the arrangement of the pharmacophoric groups in the dimer in this model.

pharmacophoric groups. This also shows that the enhancement of affinity is not due to the increase of local concentration of active peptide monomers because the mixed dimer **11** should then have an affinity similar to monomer **9** with just the glutaramide spacing unit. Additionally, the only slightly higher affinity of dimers in comparison with the monomer **8** would rather fit with a binding mode of the second peptide moiety to a subsite on the receptor than to the simultaneous binding of two identical binding pockets.[10,20]

An explanation for this behavior is revealed when the origins of the starting cyclic pentapeptide **4** and its derivatives used for dimerization are considered (Scheme 5). Both polyphemusin II and its shortened analogue T140 are rich in basic and aromatic amino acids of which the four most important residues were combined with a glycine to yield **4** (three of these residues are boxed on the left side of Scheme 5).[23] Therefore, the simplest explanation why dimerization leads to a better affinity for derivatives of polyphemusin II is that the surrounding area of the initially addressed binding pocket of **4** has additional sites for beneficial interaction with aromatic and basic groups which are addressed by the second peptide unit of the dimer with a more unspecific binding mode. This hypothesis is further supported by many other CXCR4 antagonists that typically consist of at least one basic and one aromatic moiety.[37] Therefore peptides **8** and **9** are less affine as they cannot address these other binding sites for additional beneficial interaction because of the missing second peptide unit. This binding mode with one main binding pocket and a smaller contribution to receptor affinity from the second peptide unit with a subsite differs from the binding mode of **1**. In this case, both cyclen moieties are essential for affinity as the monomer does not show any affinity.[3]

To further support this hypothesis, additional docking studies were performed. Analysis of the recently published X-ray crystal structures of CXCR4 receptor bound to an antagonist small molecule IT1t (PDB codes 3ODU, 3OE6, 3OE8, and 3OE9) and a cyclic peptide CVX15 (PDB code 3OE0) reveals that the receptor conformations are substantially identical with CVX15 occupying the great majority of the binding cleft and the low-molecular-weight IT1t ligand occupying just a portion of the same site.[19] Because the CVX15 and our compounds are both cyclic analogues of the horseshoe crab peptide polyphemusin II, molecular docking studies of the NMR solution structure of monomeric cyclopentapeptides **7** (see Experimental Procedures for further details) were attained on the structure with PDB code 3OE0.

In line with the rational design behind the synthesis of polyphemusin II-mimic small peptide **7**, the best binding pose suggested by the docking software Glide strongly resembles the experimental binding mode of CVX15 (Figure 1a).[38] In particular, the ligand Tyr^1 makes contacts with F189, Y190, and V196, while the Orn^2 residue points outward establishing an ionic interaction with D187 in extracellular loop II (ELII) (Figure 1b). The latter interaction explains why its acetylated analogue **8** and compound **9**, featuring a glutaric amide at the its side chain, are less potent binders than **7** (Table 1). Notably, the projection of Orn^2 toward the external part of the receptor is also consistent with the choice of this residue as the attachment point for the synthesis of dimeric compounds (**10**–**20**). Other important interactions are observed for Arg^3 residue, which establishes a

dx.doi.org/10.1021/jm2009716 |J. Med. Chem. 2011, 54, 7648–7662

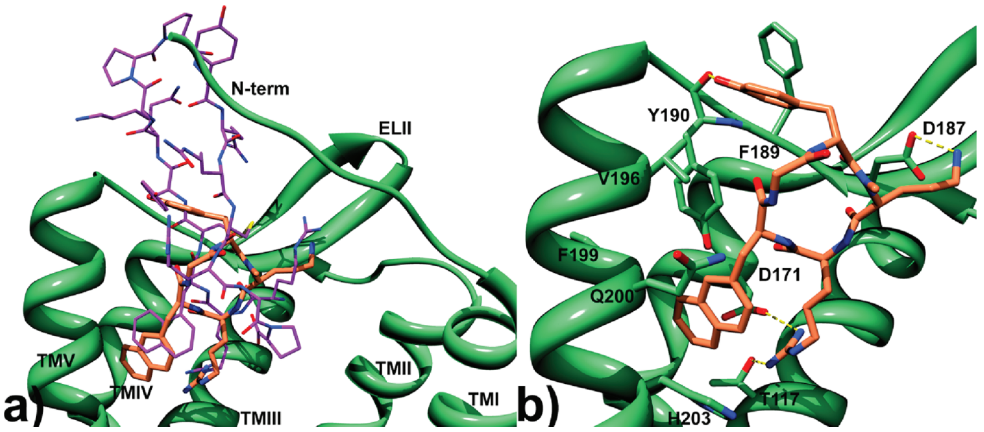

Figure 1. Binding conformation of **7** in the CXCR4 crystal structure as calculated by using Glide. The receptor is represented as light-green sticks and ribbons. The cocrystal polyphemusin analogues (a) and the ligand (a and b) are represented as magenta and orange sticks, respectively. H-bonds are represented as yellow dashed lines. For clarity reasons, only interacting residues are shown.

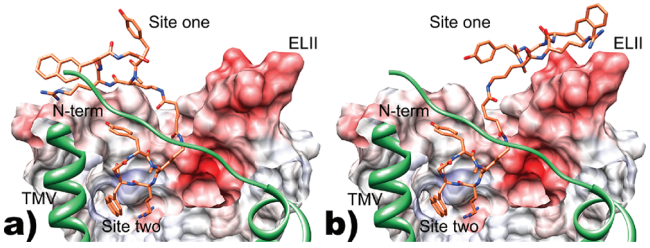

Figure 2. Alternative binding conformations (a and b) of **10** in the CXCR4 binding site. The ligand is represented as orange sticks, while receptor as light-green ribbons and a surface are colored according to its electrostatic potential from red (negative) to blue (positive).

H-bond with T117 and an ionic interaction with D171 while the adjacent Nal[4] residue is embedded in a hydrophobic pocket made up by Y190, F199, Q200, and H203 (Figure 1b).

Subsequently, molecular modeling studies were also performed to unravel the binding mode of the dimeric compounds **10**. Because the CXCR4 receptor was crystallized in a dimeric form, we first investigated whether our dimeric compounds could occupy the two binding sites of the receptor dimer. Such an hypothesis was immediately confuted by the distance between the two sites (≈ 40 Å), which cannot be spanned even by dimer **17**, which bears the longest linker. Truly, this was already suggested by the binding data, which demonstrated that compounds **10**−**20** do not bind two identical receptor clefts. The only other possibility is provided by the existence of the two neighboring binding sites in the CXCR4 monomer (namely site one and two) as previously suggested by NMR experiments and radioligand binding assays and recently confirmed by X-ray crystallography.[12,39] While site two is in the fully solved transmembrane bundle region, site one is located in the extracellular portion (N-terminus and extracellular loops), which unfortunately has been only partially solved. Thus, while the interactions of our peptides with site two can be exactly modeled, only a general picture of the binding of **10** to site one can be depicted.

Beside the above-described intrinsic difficulties, docking calculations of the dimeric ligands would be highly error prone due to the extreme flexibility of both the compounds and of the N-terminal fragment. Therefore, in our modeling studies, we started from the assumption that one cyclopentapeptide (Table 1) in compounds **10** would bind site two in the same fashion as that of the corresponding monomeric form (see above). Thus, the dimeric compound **10** was constructed starting from the calculated **7**/CXCR4 complex by adding the corresponding linker and the second cyclopentapeptide (Table 1). The built complex was then subjected to a Monte Carlo search of all the energetically feasible conformations of both the linker and peptidic portions in the receptor context. This simulation resulted in two main conformation families in which the peptide occupying site one alternatively points toward ELII, TMII, and TMII or toward TMIV and TM5 (Figure 2). In both cases, the intrinsic flexibility of the CXCR4 site one would suggest that this receptor region could plastically adapt to the different dimeric cyclopentapeptides depending on their linker length (see Table 1). Additionally, in both suggested conformations, the Arg^3 residue of the peptide occupying site one forms Coulombic interactions with negatively charged regions of the receptor, and this would be in line with SAR data, demonstrating that substitution of Arg^3 with L-citrulline leads to a loss in affinity (compound **11**).

DOTA moieties were introduced via trifunctional linkers to enable molecular imaging and endoradiotherapeutic uses. Their corresponding indium chelates were prepared as the structure of these complexes is closer to the finally desired (radio-)pharmaceuticals than the nonchelated DOTA compounds. Additionally, previous studies on CXCR4 antagonists have already shown the importance of metal ion chelates toward binding affinity in comparison with their nonchelated analogues.[16,40] All eight possible permutations of the peptide with and without an additional glycine spacer, the two linkers, as well as the free DOTA unit, and its indium chelate were synthesized and tested for their affinity (Table 2).

As expected, the dimers lose affinity through the introduction of the DOTA moiety but are suited for imaging and treatment of CXCR4 related diseases. For every pair of metal-chelated and nonchelated dimer, there is a significant difference in binding affinity showing the importance of metal ions which is often observed.[31,41] With exception of the dimers **23** and **24**, the indium chelates show better affinity, which also supports our hypothesis for the binding mode that positive charges are beneficial toward receptor binding. Furthermore, the DOTA conjugated dimers with an additional glycine spacer have the best

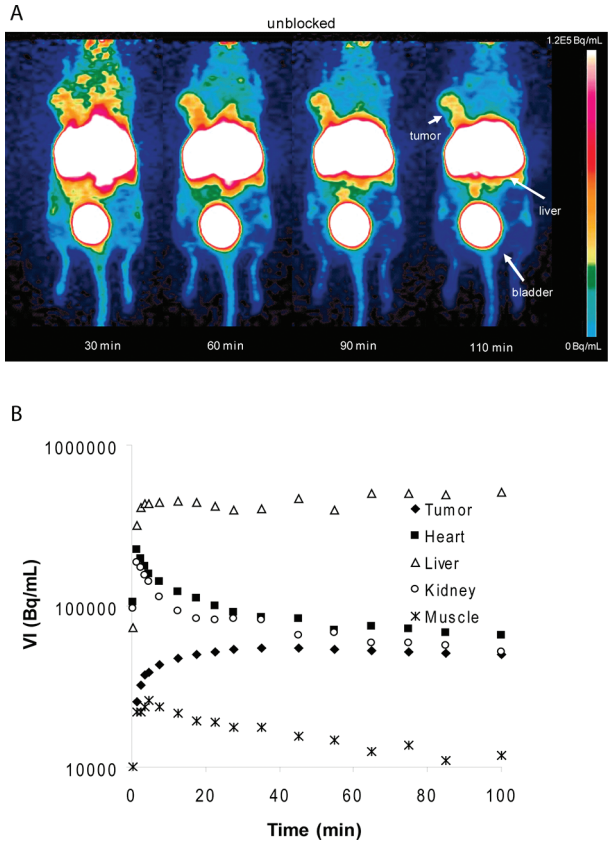

Figure 3. (A) PET dynamic imaging (0−110 min pi) of OH1 tumor bearing nude mouse using ^{68}Ga-**25**, (maximum intensity projection, MIP). (B) Time−activity curves for tumor, heart, liver, kidney, and muscle.

affinities as the distance between the two monomers corresponds to the dimer with the best affinity **15**. The affinities of the two best compounds **26** and **28** are not only about 4-fold higher than the acylated monomer **8** but they are additionally suited for imaging purposes showing the beneficial impact of the dimeric approach.

The main goal of this study was the synthesis of a library of peptides with high affinity toward CXCR4 with a view to use them as potential radiotracers for noninvasive molecular detection of primary tumors as well as targeted metastases. **25** was labeled with ^{68}Ga and evaluated in first in vivo studies in tumor bearing mice. Although a tumor uptake of up to 2% ID/g (Table 3) allowed visualization of the human tumor xenograft by PET imaging, the high liver accumulation of ^{68}Ga-**25** renders it an unsuitable radiotracer for the detection of primary tumors and their metastases, particularly in the liver and the surrounding organs (Figure 3).

In summary, we succeeded in the development of DOTA labeled multimeric peptides that bind with high affinity to CXCR4 receptors. Initial in vivo studies with a ^{68}Ga-labeled dimer for mapping CXCR4 receptors that are directly involved in organ specific metastasis allowed delineation of a CXCR4-expressing human xenograft but also demonstrated high unspecific uptake by the liver. Although this phenomenon was already observed for other radiolabeled CXCR4, ligands it is currently unclear whether this unsuitable behavior could be overcome by a further increase of the hydrophilicity of the dimer.

CONCLUSION

Starting from an acetylated monomeric CXCR4 antagonist with an IC_{50} of 60 nM, several peptidic dimers were synthesized by optimizing the distance between the monomers which enhanced the affinity 30-fold. A possible explanation for the enhanced binding affinity is a subsite binding of the second peptide unit near to the main binding pocket. This is suggested by our structural elucidation of the pharmacophoric groups in the dimers and a comparison of the dimeric structure with the 18 amino acid containing polyphemusin II, which served for the development of the original cyclic pentapeptide. This hypothesis could be further supported by molecular modeling using the recently published crystal structure of CXCR4. Eight DOTA labeled dimers were synthesized using two specially designed linker building blocks. By introduction of the DOTA moiety in combination with a metal-ion, dimers with a high potential for molecular imaging and endoradiotherapeutic purposes were designed. Subsequently ^{68}Ga-**25** was synthesized and evaluated in respect to its imaging characteristics which showed suboptimal biodistribution due to its high lipophilicity.

EXPERIMENTAL PROCEDURES

Chemicals and Instruments. All commercially available chemical reagents were used without further purification. Technical solvents were distilled before use.

Tritylchloride-polystyrene-resins (TCP resins) were purchased from PepChem and amino acid derivatives from Iris Biotech GmbH, Novabiochem, Merck, Bachem, Neosystem, and Aldrich, while all other chemicals were bought from Aldrich, Fluka, and Merck if not stated otherwise.

N-Methylpyrrolidone (NMP) was obtained from BASF and used without further distillation. Dry solvents were purchased from Aldrich, Fluka, and Merck. Dry dichloromethane was distilled from calciumhydride under argon and kept over 4 Å molecular sieve. Water for RP-HPLC was filtered through a 0.22 μm filter (Millipore, Millipak40).

RP-HPLC analyses were performed using using an Amersham Pharmacia Biotech Äkta Basic 10F equipped with an an Omnicrom YMC column (4.6 mm × 250 mm, 5 μm C_{18}, 1 mL/min). The eluent was a linear gradient from water (0.1% trifluoroacetic acid (TFA)) to acetonitrile (ACN; 0.1% TFA) over 30 min and detection at 220 and 254 nm. The retention time (R_t) of the analytical RP-HPLC is given in min, with the gradient in percentage of acetonitrile. Purities were determined at 220 nm with the Unicorn software package and are given relative to their starting compound.

Semipreparative RP-HPLC was done on a Beckman System Gold equipped with high pressure module 125, UV-detector 166, and using an Omnicrom ODS-A C18 (120 Å, 5 μm, 250 mm × 20 mm) column in combination with the same solvents as stated above.

NMR spectra were recorded on a Bruker Avance 250 or Bruker DMX 500 at 298K. The chemical shifts are reported in ppm on the δ scale relative to the solvent signal used. ^{13}C NMR-spectra were recorded using ^{1}H-broad band decoupling. Pulse programs were taken from the Bruker library or written by members of our group. Samples were prepared in tubes with a diameter of 5 mm using 0.5 mL of deuterated solvent with a final concentration of approximately 20−50 mM. The resulting spectra were processed on a workstation using Bruker TOPSPIN 1.3 software.

ESI mass spectra were recorded on a Finnigan LCQ in combination with a Agilent/HP 1100 RP-HPLC system using a Omnicrom YMC ODS-A C18 column (120 Å, 3 μm, 125 mm × 2 mm) with a flow rate of 0.2 mL/min. The eluent was a linear gradient from water to acetonitrile with 0.1% formic acid over 20 min with detection at 220 nm.

All tested compounds exhibited ≥95% purity determined with RP-HPLC-(MS).

Loading of TCP-Resin. Peptide synthesis was carried out using TCP-resin (0.9 mmol/g) following standard Fmoc-strategy. Fmoc-Xaa-OH (1.2 equiv) were attached to the TCP resin with *N*,*N*-diisopropylethylamin (DIEA; 2.5 equiv) in anhydrous DCM (0.8 mL/g resin) at room temperature for 1 h. The remaining trityl chloride groups were capped by addition of 1 mL/g (resin) of a solution of MeOH, DIEA (5:1; v:v) for 15 min. The resin was filtered and washed 5 times with DCM and 3 times with MeOH. The loading capacity was determined by weight after drying the resin under vacuum and ranged from 0.4 to 0.9 mmol/g.

On-Resin Fmoc Deprotection. The resin-bound Fmoc peptide was treated with 20% piperidine in NMP (v/v) for 10 min and a second time for 5 min. The resin was washed 5 times with NMP.

Standard Amino Acid Coupling. A solution of Fmoc-Xaa-OH (2 equiv), 2-(1*H*-benzotriazole-1-yl)-1,1,3,3-tetramethyluronium tetrafluoroborate (TBTU) (2 equiv), hydroxybenzotriazole (HOBt; 2 equiv), and DIEA (5.2 equiv) in NMP (1 mL/g resin) was added to the resin-bound free amine peptide and shaken for 60 min at room temperature and washed 5 times with NMP.

***o*-2-Nitrobenzenzesulfonyl (nosyl, *o*-Ns) Protection.** A solution of *o*-Ns-Cl (5 equiv) and collidine (10 equiv) in NMP (1 mL/g resin) was added to the resin-bound free amine peptide and shaken for 15 min at room temperature. The resin was washed 3 times with NMP and 3 times with dry THF.

***N*-Methylation under Mitsunobu Conditions.** A solution of triphenylphosphine (5 equiv), diisopropyl azodicarboxylate (DIAD; 5 equiv) and MeOH (10 equiv) in dry THF (1 mL/g resin) was added to the resin-bound *o*-Ns protected peptides and shaken for 10 min at room temperature. The resin was filtered off and washed 3 times with dry THF and 3 times with NMP.

On-Resin *o*-Ns Deprotection. For *o*-Ns deprotection, the resin-bound *o*-Ns-peptides were stirred in a solution of mercaptoethanol (10 equiv) and DBU (5 equiv) in NMP (1 mL/g resin) for 5 min. The deprotection procedure was repeated one more time, and the resin was washed 5 times with NMP.

Amino Acid Coupling to Hindered Amines. A solution of Fmoc-Xaa-OH (2 equiv), 2-(7-aza-1*H*-benzotriazole-1-yl)-1,1,3,3-tetramethyluronium hexafluorophosphate (HATU; 2 equiv), 1-hydroxy-7-azabenzotriazole (HOAt; 2 equiv), and DIEA (4 equiv) in NMP (1 mL/g resin) was added to the resin-bound peptides and shaken for 3 h at room temperature and washed 5 times with NMP.

Allyloxycarbonyl (Alloc) and Allyl Deprotection. $Pd(PPh_3)_4$ (0.125 equiv) in dry DCM (0.5 mL/g resin) was added to the resin-bound Alloc peptide followed by an addition of phenylsilane in dry DCM (0.5 mL/g resin) and shaken for 1 h. The resin was washed 5 times with DCM.

Peptide Cleavage from the Resin. For complete cleavage of the peptides from the resin, they were treated three times with a solution of DCM and hexafluoroisopropanol (HFIP; 4:1; v:v) at room temperature for half an hour and the solvent evaporated under reduced pressure.

Cyclization. To a solution of peptide in DMF (1 mM peptide concentration) and $NaHCO_3$ (5 equiv) diphenylphosphoryl azide (DPPA; 3 equiv) was added at room temperature (RT) and stirred overnight or until no linear peptide could be observed by ESI-MS. The solvent was evaporated to a small volume under reduced pressure and the peptides precipitated in saturated NaCl solution and washed two times in HPLC grade water.

Dimerization by Acylation in Solution. Fully deprotected peptides were stirred with HATU (1.1 equiv) and DIEA (2.2 equiv) and the corresponding acid (1 equiv) in DMF (10 mM peptide concentration) for 30 min at RT. The solution was directly purified by HPLC separation.

Removal of Acid Labile Side Chain Protecting Groups. Cyclized peptides were stirred in a solution of TFA, water, and TIPS (95:2.5:2.5) at RT for 1 h or until no more protected peptide could be observed by ESI-MS and precipitated in diethylether and washed two more times.

Removal of DOTA *t*-Bu Groups. To the coupling solution with the dimerized peptides the same volume of conc HCl was added on an ice bath under vigorous stirring. The deprotection was carried out at RT and monitored for completeness by ESI-MS every 30 min and stopped by neutralizing with conc NH_4OH on an ice bath.

Chelation of Indium with DOTA Ligands. The solution with the deprotected DOTA-dimers was treated with $InCl_3$ (5 equiv) dissolved in 5 M aqueous NH_4Cl of the same volume as the total deprotection solution. After 15 min of stirring at RT, the solution was subjected to HPLC purification.

Receptor Binding Assays. Competition studies were performed on Jurkart cells using *cyclo*(-D-Tyr^1[^{125}**I**]-Arg^2-Arg^3-Nal^4-Gly^5) (^{125}I-CPCR4) as radioligand. In brief, cells were resuspended in PBS/0.2% BSA. A total of 200 μL of the suspension containing 400000 Jurkat cells were incubated with 25 μL of the tracer solution (containing 3.1 kBq, approximately 0.1 nM) and 25 μL of the test peptides at different concentrations of 10^{-11} to 10^{-5} M. Nonspecific binding was determined in the presence of 1 μM cold *cyclo*(-D-Tyr^{1}Arg^2-Arg^3-Nal^4-Gly^5). After shaking for 2 h at RT, the incubation was terminated by centrifugation at 1300 rpm for 5 min. Cell pellets were washed twice with cold PBS. Cell bound radioactivity was determined by using a 1480 Wizard3 gamma-counter from Wallac (Turku, Finland). Experiments were repeated 2−3 times in triplicate. IC_{50} values of the compounds were calculated by nonlinear regression using GraphPad Prism (GraphPad Prism 4.0 Software, Inc., San Diego, CA, USA). Each data point is the average of three determinations.

Labeling with ^{68}Ga. ^{68}Ga-**25** was selected for an initial in vivo study. For this purpose, Gallium-68 (ϵ^+ = 89%, $t_{1/2}$ = 68.1 min, $E_{\beta+\max}$ = 1.90 MeV) was eluted from a commercially available Ge-68/Ga-68 generator (iThemba, South Africa) by diluted HCl. The fraction with the highest activity, approximately 1.2 mL with >80% of the entire eluted activity, was used for labeling of **25** using a commercially available fully automated labeling module (Gallelut-Synthesizer, Scintomics GmbH, Fürstenfeldbruck, Germany). After the pH of the eluate was adjusted with a suitable amount of HEPES (4-(2-hydroxyethyl)-1-piperazineethanesulfonic acid) (930 μL, 600 mg HEPES/0.5 mL H_2O), 35 μg (15 nmol) of the peptide was added. After reaction for 5 min at 95 °C, quality control of the product was carried out by radio thin layer chromatography (TLC) on Silica gel 60-plates using 0.5 μL of product solution on two different TLC systems: (a) eluent TLC-1, 0.1 M sodium citrate (5.89 g trisodium citrate dihydrate in 200 mL ultrapure water); eluent TLC-2, (1/1, v/v) methanol/1 M ammonium acetate (15.46 g ammonium acetate in 200 mL ultrapure water). Using the TLC method 1, the product and Ga-colloid stay at the starting point, whereas free Ga^{3+} moves with front. Using the TLC method 2, uncomplexed Ga-species stay at starting point, whereas the labeled peptide moves with the front. The quality control of the labeled peptide was also achieved by RP-HPLC. HPLC analysis was performed on a Semi RP18 Multosphere Column (250 mm × 100 mm) applying a linear gradient system at a 5 mL/min flow rate from 49% B to 60% B in 20 min, where solvent A = aqueous ammonium formate 0.2 M and solvent B = MeOH. The detection of the peptides was performed via a UV detector at 220 nm.

Biosdistribution Studies. Athymic nude mice (approximately 30 g) were obtained from Charles River, Germany. The animals were inoculated subcutaneously into the right flank with OH1 h-SCLC cells (5×10^6 cells/animal). Tumors were allowed to grow for three weeks. Tissue distribution studies of the ^{68}Ga labeled tracer carried out after the intravenous administration of 0.1 mL [~70 μCi (~2.6 MBq), 0.7 μg of total peptide] of the radiolabeled product via the tail vein and the

animals (n = 5) were sacrificed 1 h pi. Subsequently, the tissues and organs were weighted, the radioactivity was counted in a 1480 Wizard3 gamma-counter from Wallac (Turku, Finland), and the % ID/g of each organ or tissue was calculated. Specificity of binding was demonstrated by coinjection of a ^{nat}Ga-tracer (compound **2c**, ref 31) (100 μg/mouse; n = 1).[31]

PET-Camera Imaging. Mice (~30 g) were anaesthetized using isoflurane anesthesia and injected with 80−90 μCi (~3 MBq, 1.4 μg of total peptide) of ^{68}Ga-**25** via the tail vein in a volume of 300 μL of PBS. For the blocking experiments, mice were coinjeced with 50 μL (100 μg) of ^{nat}Ga-tracer (compound **2c**, ref 31) complex in a total volume of 300 μL. PET scans were performed using an Inveon Siemens PET scanner, and dynamic imaging was performed immediately after the time of injection with acquisition times: 5 × 60 s, 5 × 300 s, 6 × 600 s, 1 × 120 s, and a total duration being 110 min (Figure 3A). Analysis of tracer kinetics was performed by drawing a circular region of interest (ROI) in the tumor, heart, liver, kidney, and muscle. The average of the accumulated radioactivity in the ROI was calculated in Bq/mL and time activity curves were plotted, representing the radioactivity in the organs of interest versus time (Figure 3B). For blocking experiments, dynamic images were obtained using acquisition times of 5 × 60 s, 5 × 300 s, and 1 × 600 s, with a overall sorter imaging period of 40 min. All images were reconstructed by a two-dimensional ordered subsets expectation maximum (2D-OSEM) algorithm, and no correction was applied for attenuation. Images analysis was done using Inveon software. The results were calculated as Bq/mL.

Solution Synthesis. *General Amine Protection Procedure.* To a 0.2 M solution of amino acid and Na_2CO_3 (0.5 M), the same volume of a 0.2 M reagent solution in THF was added and stirred at RT for 1 h. The THF was evaporated under reduced pressure, the aqueous phase washed once with diethylether and acidified with conc HCl to pH 1, and the product extracted with EtOAc. The combined organic layers were dried (Na_2SO_4), filtered, concentrated, and dried in vacuo.

Boc Deprotection. First 3−8 mmol of Boc protected amino acid were dissolved in 10 mL of DCM and 5 mL of TFA added slowly. Then the solution was stirred at RT for 45 min and the solvent evaporated in vacuo to yield the crude product ready for reprotection.

N^{α}-Ns-N^{δ}-Boc-D-Ornithine. N^{δ}-Boc-D-ornithine (1.51 g, 6.5 mmol) was protected with *o*-nitrobenzenesulfonylchloride (NsCl) (1.44 g, 6.5 mmol) and gave a slightly yellow, sticky oil as sufficiently pure product (2.43 g, 90%). ^{1}H NMR (250 MHz, DMSO-d_6): δ 12.72 (s, 1H), 8.46 (d, 1H), 8.01 (m, 1H), 7.93 (m, 1H), 7.86 (m, 2 H), 6.78 (t, 1 H), 3.85 (m, 1H), 2.85 (m, 2 H), 1.38 (m, 13H). ^{13}C NMR (125 MHz, DMSO-d_6): 172.3, 147.7, 134.4, 133.8, 132.9, 130.3, 124.5, 110.7, 77.9, 56.2, 29.7, 28.7, 26.4. R_t (10−100%): 18.6 min. m/z calcd for $C_{16}H_{23}N_3O_8S$, 417.12; found, 440.1 [M + Na$^+$].

N^{α}-Alloc-N^{δ}-Boc-D-Ornithine. N^{δ}-Boc-L-ornithine (0.49 g, 2.1 mmol) was protected with allyl chloroformate (0.22 mL, 2.1 mmol) and gave a slightly yellow, sticky oil as sufficiently pure product (0.53 g, 80%). ^{1}H NMR (250 MHz, DMSO-d_6): δ 12.52 (s, 1H), 7.49 (d, 1H), 6.78 (t, 1H), 5.91 (br m, 1H), 5.30 (dd, 1 H), 5.19 (dd, 1 H), 4.48 (m, 2H), 3.91 (br m, 1H), 2.91 (m, 2H), 1.81−1.40 (br m, 4H), 1.38 (s, 9H). ^{13}C NMR (63 MHz, DMSO-d_6): 174.4, 156.5, 156.1, 134.1, 117.4, 77.9, 65.1, 60.2, 54.1, 28.8, 26.7, 14.6. R_t (10−100%): 16.7 min. m/z calcd for $C_{14}H_{24}N_2O_6$, 316.16; found, 339.3 [M + Na$^+$].

N^{α}-Alloc-N^{δ}-Fmoc-D-Ornithine. N^{α}-Alloc-N^{δ}-Boc-D-ornithine (0.36 g, 1.68 mmol) was subjected to Boc deprotection and subsequently reprotected with Fmoc-OSu (0.567 g, 1.68 mmol) and gave a white foam as sufficiently pure product (0.61 g, 89%). ^{1}H NMR (500 MHz, DMSO-d_6): δ 12.5 (s, 1H,), 7.9 (d, 2H), 7.7 (d, 2H), 7.5 (d, 1H), 7.4 (t, 2H), 7.32 (t, 2H), 7.28 (m, 1H), 5.9 (m, 1H), 5.3 (d, 1H), 5.2 (d, 1H), 4.5 (d, 2H), 4.3 (d, 2H), 4.2 (t, 1H), 3.9 (m, 1H), 3.0 (d, 2H), 1.7 (m, 1H), 1.5 (m, 3H). ^{13}C NMR (125 MHz, DMSO-d_6): 174, 156.0, 155.9, 144, 141, 133, 128, 127.0, 126.9, 125.1, 125.0, 120.1, 119.9, 65, 64, 53.54, 53.50, 47, 28, 26. R_t (10−100%): 21.9 min. m/z calcd for $C_{24}H_{26}N_2O_6$, 438.18; found, 461.5 [M + Na$^+$].

(9H-Fluoren-9-yl)methyl (R)-1-(Carbonyl)-3-(tert-butoxycarbonyl)-propan-2-ylcarbamate. The product was obtained similar to a general procedure given in literature.[35] N^{α}-Fmoc-aspartic acid(tBu)OH (2.0 g; 4.9 mmol; 1equiv) was dissolved in anhydrous THF (20 mL). NEt_3 (0.74 mL; 5.4 mmol; 1.1 equiv) and ethylchloroformate (0.52 mL; 5.4 mmol; 1.1 equiv) were added sequentially at −15 °C. Stirring was continued for 15 min, and then the solution was allowed to warm up to 0 °C. In the meantime, *N*-methylnitrosourea (2.5 g; 24.3 mmol; 5 equiv) was stirred in ice-cold Et_2O (20 mL) and 40% KOH (20 mL; ice-cold) was added dropwise until complete dissolution. The yellow diazomethane solution in Et_2O was added dropwise at 0 °C to the amino acid solution, and it was then allowed to warm up to RT and stirred for another 2.5 h. Excess diazomethane was decomposed by dropwise addition of HOAc. The solution was washed with satd $NaHCO_3$, satd NH_4Cl, and brine. The organic layer was dried (Na_2SO_4) and evaporated under reduced pressure. The resulting diazo ketone was dissolved in water/dioxane (1:5; v/v; 160 mL). After addition of silver benzoate (0.12 g; 0.5 mmol; 0.1 equiv), the mixture was sonicated in an ultrasound bath until complete conversion (30 min) monitored by TLC (MeOH/DCM, 1:20; R_f, 0.1−0.2). After evaporation of dioxane under reduced pressure, the solution was acidified with 5% HCl and the precipitate extracted with EtOAc (three times). The organic layer was dried (Na_2SO_4) and evaporated under reduced pressure and the crude product purified by flash chromatography (MeOH/DCM, 1:20; R_f, 0.1−0.2) to yield 1.3 g (3.1 mmol; 63% yield). ^{1}H NMR (250 MHz, DMSO-d_6): δ 12.2 (s, br, 1H,), 7.90 (d, 2H), 7.69 (dd, 2H), 7.42 (t, 2H), 7.33 (m, 3H), 4.27 (m, 3H), 3.59 (m, 1H), 2.41 (m, 4H), 1.38 (s, 9H). ^{13}C NMR (75 MHz, DMSO-d_6): 172.49, 170.24, 144.35, 141.19, 128.07, 127.51, 125.63, 120.56, 80.39, 65.80, 60.20, 47.17, 45.81, 28.13. R_t (10−100%): 23.5 min. m/z calcd for $C_{24}H_{27}NO_6$, 425.18; found, 448.1 [M + Na$^+$].

(9H-Fluoren-9-yl)methyl (R)-1-((Allyloxy)carbonyl)-3-(tert-butoxycarbonyl)propan-2-ylcarbamate. The product was obtained similar to a procedure given in literature.[42] (9*H*-Fluoren-9-yl)methyl (*R*)-1-(carbonyl)-3-(*tert*-butoxycarbonyl)propan-2-ylcarbamate (0.98 g; 2.3 mmol; 1 equiv) was stirred with allyl bromide (5.52 mL; 6.4 mmol; 2.8 equiv) and DIEA (0.78 mL; 4.6 mmol; 2 equiv) in ACN (4.6 mL) at 45 °C for 1 h. The reaction was monitored by TLC MeOH/DCM (1:20; v/v). The solution was allowed to reach RT. After addition of ethylacetate (EtOAc; 20 mL), the organic layer was washed with satd $KHSO_4$, satd $NaHCO_3$, and half-satd NaCl, dried (Na_2SO_4), and evaporated under reduced pressure to yield 0.77 g (1.7 mmol; 74% yield). ^{1}H NMR (250 MHz, $CDCl_3$): δ 7.76 (d, 2H,), 7.58 (d, 2H), 7.40 (t, 2H), 7.31 (m, 2H), 5.91 (m, 1H), 5.63 (d, 1H), 5.32 (m, 1H), 5.24 (d, 1H), 4.60 (d, 2H), 4.36 (m, 3H), 4.21 (m, 1H), 2.66 (m, 4H), 1.45 (s, 9H). ^{13}C NMR (75 MHz, $CDCl_3$): 143.91, 141.29, 131.84, 127.67, 127.04, 125.08, 119.95, 118.57, 66.86, 65.38, 47.21, 45.13, 39.26, 38.08, 28.05. R_t (10−100%): 27.6 min. m/z calcd for $C_{27}H_{31}NO_6$, 465.22; found, 488.3 [M + Na$^+$].

(9H-Fluoren-9-yl)methyl (S)-1-((Allyloxy)carbonyl)-3-(carbonyl)propan-2-ylcarbamate. The product was obtained similar to a procedure given in literature.[42] (9*H*-Fluoren-9-yl)methyl (*R*)-1-((allyloxy)carbonyl)-3-(*tert*-butoxycarbonyl)propan-2-ylcarbamate (0.77 g; 1.65 mmol) was dissolved in DCM (4 mL), and TFA (2 mL) was added and stirred for 2 h at RT. After evaporation to dryness, the solid was dissolved in satd $NaHCO_3$, washed with ether, and acidified (pH 2) with HCl (5%) to form a white precipitate that was extracted two times with EtOAc. The organic layer was washed with acidified water (HCl, pH 1), dried (Na_2SO_4), and evaporated under reduced pressure to yield 0.58 g (1.4 mmol; 85% yield). ^{1}H NMR (250 MHz, $CDCl_3$): δ 7.75 (d, 2H,), 7.68 (s, 1H), 7.57 (d, 2H), 7.40 (t, 2H), 7.31 (m, 2H), 5.89 (m, 1H), 5.66 (d, 1H), 5.28 (m, 2H), 4.60 (d, 2H), 4.38 (m, br, 2H), 4.22 (m, 1H), 2.62

(m, 4H). ^{13}C NMR (75 MHz, $CDCl_3$): 143.69, 141.33, 131.60, 127.77, 127.10, 125.00 120.01, 118.87, 67.25, 65.65, 47.13, 44.47, 37.87, 37.64. R_t (10−100%): 22.0 min. m/z calcd for $C_{23}H_{23}NO_6$, 409.15; found, 432.2 [M + Na^+].

N^{α}-Fmoc-L-aspartic Acid (t-Bu) Allylester. The product was obtained similar to a procedure given in literature.[43] N^{α}-Fmoc-L-aspartic acid (β-*t*-Bu ester) (0.103 g; 2.50 mmol; 1equiv) was stirred with allyl bromide (6.0 mL; 7.0 mmol; 2.8 equiv) and DIEA (0.78 mL; 5.0 mmol; 2 equiv) in ACN (5.0 mL) at 45 °C for 100 min. The reaction was monitored by TLC MeOH/DCM (1:20; v/v). The solution was allowed to reach RT. After addition of EtOAc (40 mL), the organic layer was washed with satd $KHSO_4$, satd $NaHCO_3$, and half-satd NaCl, dried (Na_2SO_4), and evaporated under reduced pressure to yield 1.01 g (2.24 mmol; 90% yield). ^{1}H NMR (250 MHz, $CDCl_3$): δ 7.74 (d, 2H,), 7.58 (m, 2H), 7.38 (t, 2H), 7.29 (t, 2H), 5.89 (m, 1H), 5.81 (d, 1H), 5.32 (d, 1H), 5.23 (d, 1H), 4.56 (m, 3H), 4.37 (m, 3H), 4.23 (m, 1H), 2.86 (m, 2H), 1.42 (s, 9H). ^{13}C NMR (75 MHz, $CDCl_3$): 170.62, 170.00, 155.98, 143.91, 143.73, 141.29, 131.49, 127.71, 127.07, 125.13, 119.98, 118.80, 81.89, 67.28, 66.30, 50.61, 47.10, 37.79, 28.03. R_t (10−100%): 27.8 min. m/z calcd for $C_{26}H_{29}NO_6$, 451.20; found, 474.3 [M + Na^+].

N^{α}-Fmoc-L-aspartic Acid (OH) Allylester. The product was obtained similar to a procedure given in literature.[43] N^{α}-Fmoc-L-aspartic acid (β-*t*-Bu) allylester (1.01 g; 2.23 mmol) was dissolved in DCM (4 mL), and TFA (2 mL) was added and stirred for 1 h at RT. After evaporation to dryness, the solid was dissolved in satd $NaHCO_3$, washed with ether, and acidified (pH 2) with HCl (5%) to form a white precipitate that was extracted two times with EtOAc. The organic layer was washed with acidified water (HCl, pH 1), dried (Na_2SO_4), and evaporated under reduced pressure to yield 0.77 g; 1.94 mmol; 87% yield. ^{1}H NMR (250 MHz, DMSO): δ 7.90 (m, 2H,), 7.83 (m, 1H), 7.70 (d, 2H), 7.42 (m, 2H), 7.32 (m, 2H), 5.87 (m, 1H), 5.30 (d, 1H), 5.18 (m, 1H), 4.58 (d, 2H), 4.45 (m, 1H), 4.26 (m, 3H), 2.70 (m, 2H). ^{13}C NMR (75 MHz, $CDCl_3$): 171.85, 171.29, 144.22, 141.20, 132.72, 128.11, 127.540, 125.66 120.59, 118.03, 66.24, 65.52, 51.02, 47.07, 36.32. R_t (10−100%): 22.0 min. m/z calcd for $C_{22}H_{21}NO_6$, 395.14; found, 418.1 [M + Na^+].

Glutaric Acid Mono Amide (Sodium Salt). The ammonium salt was synthesized via a modified protocol found in literature and then replaced with sodium ions.[44] Glutaric anhydride (0.50 g; 4.4 mmol) was dissolved in DCM (10 mL) and insoluble glutaric acid filtered off. Aqueous ammonium hydroxide was heated to 70 °C and the gas bubbled through the stirred DCM solution. After precipitation of a white solid, the ammonia was heated for another 30 min and the DCM solution stirred overnight. The white solid was filtered, washed two times with DCM (10 mL), and dried to yield 0.58 g (3.9 mmol; 89%) of glutaric acid mono amide ammonium salt. The ammonium salt was dissolved in water (10 mL) and treated with an equimolar amount of sodium hydroxide (0.16 g) and lyophilized to yield the sodium salt. ^{1}H NMR (250 MHz, DMSO-d_6): δ 7.31 (s, 1H,), 6.63 (s, 1H), 2.03 (q, 4H), 1.65 (m, 2H).

1,4,7-Tris(tert-butoxycarbonylmethyl)-1,4,7,10-tetraazacyclododecane-10-acetic Acid. (Tris(*t*-Bu)DOTA) was synthesized according to procedures given in the literature.[45]

NMR Spectroscopy and Computational Studies. *NMR Spectroscopy.* Nuclear magnetic resonance (NMR) experiments were recorded with a 20 mM concentrated sample in aqueous 50 mM acetate buffer pH 4.5 at 280K on a Bruker DMX600 spectrometer (Bruker Biospin, Rheinstetten, Germany). Spectra were referenced relative to external DSS.[46] Water suppression was achieved with a WATERGATE sequence.[47] ^{1}H,^{1}H-TOCSY (80 ms mixing time) and ^{1}H,^{1}H−COSY experiments were used for chemical shift assignment of all proton resonances using standard procedures.[48] Sequential assignment was accomplished by throughbond connectivities from heteronuclear multibond correlation (HMBC) spectra.[49] The ^{1}H,^{1}H E-COSY experiment was used for the extraction of homonuclear coupling constants.[50] For the extraction of distance information, ROESY experiments (150 ms mixing time) were recorded. 8k and 512 data points were recorded in the direct and indirect dimension, respectively.[51] For the E-COSY experiment, 2k data points were recorded in the indirect dimension.

Molecular Dynamics Simulation. The GROMACS 4.0.3[52] software package (www.gromacs.org), was used to perform the MD simulations. All scripts for subsequent analysis were packaged with GROMACS. The OPLS-AA force field was used for the molecular dynamic simulations. Rigid SPC water was the water model used. Remaining solute bonds were constrained by the SHAKE algorithm and temperature and pressure control was executed by Berendsen coupling.[53] A cubic simulation box with periodic boundary conditions was employed, along with PME ($r_{coulomb}$ = 1.1 nm) for electrostatic and with a cut-off distance (r_{vdw} = 1.1 nm) for Lennard-Jones nonbonding interactions. All of the MD simulations were established and performed using the following procedure. The molecules were built with SYBYL (SYBYL 7.3, Tripos International, 1699 South Hanley Rd., St. Louis, Missouri 63144, USA), placed at the center of a cubic simulation box, and a steepest descent energy minimization in vacuo was conducted. The box was then solvated with water molecules. Steepest decent energy minimization was used to remove bad van der Waals contacts between atoms. This was followed by a series of equilibration steps of 50 fs starting at 50 K (position restraints at 250000) and going in 50 K steps toward 300 K (no position restraints) while lowering the position restraints in each step by a factor of 10 except for the last step, where it was lowered by a factor of 25. These short simulation was performed with temperature coupling (τT = 0.1 ps; T_{ref} is equal to the simulated temperature) and no pressure coupling and used the output of the previous step as input. An additional equilibration step at 300 K with temperature coupling (τT = 0.1 ps; T_{ref} = 300 K) and isotropic pressure coupling (τP = 0.5 ps with reference pressure of 1.01325 bar and 4.5 × 10^{-5} compressibility) was done for 100 fs. Following the short equilibrations the long simulations for analysis were run for a total simulation time of 100−150 ns with otherwise the same specifications as the last equilibration step.

Docking. The crystal structure with PDB code 3OE0 was downloaded from the RCSB Protein Data Bank.

This file contains a single unit of the CXCR4 receptor cocrystallized with the cyclic peptide CVX15, which is structurally similar with the cyclopentapeptides antagonist used in this study. The 3OE0.pdb crystal structure was prepared using the "Protein Preparation Wizard" panel of Schrödinger 2010 molecular modeling package.[54] In particular, using the "preprocess and analyze structure" tool, the bond orders were assigned, all the hydrogen atoms were added, the disulfide bonds were assigned, and all the water molecules in a distance greater than 5 Å from any heterogroup were deleted. Using Epik 2.0 a prediction of the heterogroups ionization and tautomeric states was performed.[54] An optimization of the hydrogen-bonding network was performed using the "H-bond assignment" tool. Finally, using the "impref utility", the positions of the hydrogen atoms were optimized by keeping all the heavy atoms in place.

Glide is a grid-based ligand docking with energetics approach and searches for favorable interactions between ligands and receptors. The shape and properties of the receptor are represented on a grid by different sets of fields that provide progressively more accurate scoring of the ligand pose. These fields are generated as preprocessing steps in the calculation and hence need to be computed only once for each receptor. For the grid generation of the CXCR4 receptor, the binding site was defined using the native CVX15 ligand cocrystallized with the receptor. This box gives a more precise measure of the effective size of the search space. However, ligands can move outside this box during grid minimization. The Cartesian coordinates of the inner box, *X*, *Y*, and *Z* length were set to 30 Å.

These grids were used to dock both the *trans* and *cis* conformations of peptide **7** as experimentally determined by NMR, distance geometry, and subsequent molecular dynamics (restrained MD). The

conformational space of the ligand is defined by Glide by several lowest-energy poses that are subjected to a Monte Carlo procedure that examines nearby torsional minima. This procedure is needed in some cases to properly orient peripheral groups and occasionally alters internal torsion angles. The default value (1.00) for the van der Waals radii scaling factor was chosen, which means no scaling for the nonpolar atoms was performed (no flexibility was simulated for the receptor). In the present study, the extra-precision (XP) mode of GlideScore function was used to score the obtained binding poses. The force field used for the docking was the OPLS-2005.[55]

Conformational Search. The **7**/CXCR4 complex obtained from docking studies was used as a starting point to build the **10**/CXCR4 complex, which was then subjected to conformational sampling calculations. In particular, the structure of **10** was built and optimized with MacroModel within the Schrödinger Maestro package, keeping also the second cyclopentapeptide in its *trans* conformation. Macromodel supplies eight search algorithms: torsional sampling, serial torsional sampling, systematic torsional sampling, mixed torsional/low-mode sampling, low-mode sampling, serial low-mode sampling, large-scale low-mode sampling, and mixed torsional/large-scale low-mode sampling. Among them, the large-scale low-mode sampling method was used as it implements techniques to reduce the memory requirements so that it can be applied to large systems such as protein−ligand complexes. The calculations were performed with OPLS-2005 force field in a water solvent model. The energy window for saving structures was set to 5.02 kcal/mol. Each conformational search included 10000 iterations. The rmsd cutoff value was set at 0.5 Å to avoid retrieving redundant conformations. When each search was finished, 100 representative ligand/receptor conformations were retained by the ligand heavy-atom rmsd analysis. In this way, lower energy and relatively diverse ligand conformation ensembles were generated. Pictures of the modeled ligand/receptor complexes were rendered with the UCSF Chimera package from the Resource for Biocomputing, Visualization, and Informatics at the University of California, San Francisco.[56]

■ ASSOCIATED CONTENT

Supporting Information. Experimental details and characterization data of synthesized compounds and bioconjugates. This material is available free of charge via the Internet at http://pubs.acs.org.

■ AUTHOR INFORMATION

Corresponding Author

*Phone: ++49 + 89/289-13300. Fax: ++49 + 89/289-13210. E-mail: Kessler@tum.de. Address: Institute for Advanced Study, Technische Universität München, Lichtenbergstrasse 2a, D-85748 Garching, Germany.

■ ACKNOWLEDGMENT

We thank M. Wolff and B. Cordes, both Department Chemie and M. Beschorner, A. Alke, K. McGuire, S. Reder, Dr. M. Schottelius, and Dr. J. Notni, all Lehrstuhl für Pharmazeutische Radiochemie, for their assistance. Part of this work was supported by the Center of Integrated Protein Science Munich (CIPS), the Federal Ministry of Education and Research (MOBITEC/MOBITUM 01EZ0826), and the German Research Foundation (SFB 824/1-2009).

■ ABBREVIATIONS USED

AA, amino acid; D-[*N*Me]Orn, N^{α}-methyl-D-ornithine; DIAD, diisopropylazodicarboxylate; DIEA, diisopropylethylamine; DPPA, diphenylphosphoric acid azide; DOTA, (1,4,7,10-tetraazacyclododecane-1,4,7,10-tetraacetic acid); GPCR, G-protein coupled receptor; HATU, *O*-(7-Azabenzotriazol-1-yl)-*N*,*N*,*N*′,*N*′,-tetramethyluroniumhexafluorophosphat; HFIP, hexafluoroisopropanol; HIV, human immunodeficiency virus; HOAt, 1-hydroxy-7-azabenzotriazol; HOBT, 1-hydroxybenzotriazol; MIP, maximum intensity projection; Nal, L-3-(2-naphthyl)alanine; NMP, *N*-methyl-2-pyrrolidone; NMR, nuclear magnetic resonance; Ns, N^{α}-2-nitrobenzenesulfonyl; NsCl, N^{α}-2-nitrobenzenesulfonylchloride; PET, positron emission tomography; SPPS, solid phase peptide synthesis; TBTU, *O*-(1*H*-benzotriazol-1-yl)-*N*,*N*,*N*′,*N*′-tetramethyluroniumtetra-fluoroborate; TFA, trifluoroacetic acid; TIPS, triisopropylsilane

■ REFERENCES

(1) (a) Nagasawa, T.; Kikutani, H.; Kishimoto, T. Molecular cloning and structure of a pre-B-cell growth-stimulating factor. *Proc. Natl. Acad. Sci. U.S.A.* **1994**, *91*, 2305–2309. (b) Oberlin, E.; Amara, A.; Bachelerie, F.; Bessia, C.; Virelizier, J. L.; Arenzana-Seisdedos, F.; Schwartz, O.; Heard, J. M.; Clark-Lewis, I.; Legler, D. F.; Loetscher, M.; Baggiolini, M.; Moser, B. The CXC chemokine SDF-1 is the ligand for LESTR/fusin and prevents infection by T-cell-line-adapted HIV-1. *Nature* **1996**, *382*, 833–835. (c) Tashiro, K.; Tada, H.; Heilker, R.; Shirozu, M.; Nakano, T.; Honjo, T. Signal Sequence Trap—A Cloning Strategy for Secreted Proteins and Type-I Membrane-Proteins. *Science* **1993**, *261*, 600–603. (d) Bleul, C. C.; Farzan, M.; Choe, H.; Parolin, C.; Clark-Lewis, I.; Sodroski, J.; Springer, T. A. The lymphocyte chemoattractant SDF-1 is a ligand for LESTR/fusin and blocks HIV-1 entry. *Nature* **1996**, *382*, 829–833. (e) Busillo, J. M.; Benovic, J. L. Regulation of CXCR4 signaling. *Biochem. Biophys. Acta: Biomembranes* **2007**, *1768*, 952–963. (f) Burger, M.; Hartmann, T.; Krome, M.; Rawluk, J.; Tamamura, H.; Fujii, N.; Kipps, T. J.; Burger, J. A. Small peptide inhibitors of the CXCR4 chemokine receptor (CD184) antagonize the activation, migration, and antiapoptotic responses of CXCL12 in chronic lymphocytic leukemia B cells. *Blood* **2005**, *106*, 1824–1830. (g) Murdoch, C. CXCR4: chemokine receptor extraordinaire. *Immunol. Rev.* **2000**, *177*, 175–184. (h) Klein, R. S.; Rubin, J. B. Immune and nervous system CXCL12 and CXCR4: parallel roles in patterning and plasticity. *Trends Immunol.* **2004**, *25*, 306–314.

(2) (a) Tamamura, H.; Fujii, N. The therapeutic potential of CXCR4 antagonists in the treatment of HIV infection, cancer metastasis and rheumatoid arthritis. *Expert Opin. Ther. Targets* **2005**, *9*, 1267–1282. (b) De Clercq, E. New approaches toward anti-HIV chemotherapy. *J. Med. Chem.* **2005**, *48*, 1297–1313. (c) Tsutsumi, H.; Tamamura, H.; Fujii, N. Inhibitors of the chemokine receptor CXCR4: Chemotherapy of AIDS, metastatic cancer, leukemia and rheumatoid arthritis. *Lett. Drug Des. Discovery* **2007**, *4*, 20–26.

(3) De Clercq, E. Potential clinical applications of the CXCR4 antagonist bicyclam AMD3100. *Mini-Rev. Med. Chem.* **2005**, *5*, 805–824.

(4) Burger, J. A.; Kipps, T. J. CXCR4: a key receptor in the crosstalk between tumor cells and their microenvironment. *Blood* **2006**, *107*, 1761–1767.

(5) Wong, D.; Korz, W. Translating an antagonist of chemokine receptor CXCR4: from bench to bedside. *Clin. Cancer Res.* **2008**, *14*, 7975–7980.

(6) (a) Khan, A.; Greenman, J.; Archibald, S. J. Small molecule CXCR4 chemokine receptor antagonists: developing drug candidates. *Curr. Med. Chem.* **2007**, *14*, 2257–2277. (b) Levesque, J. P.; Winkler, I. G. Mobilization of hematopoietic stem cells: state of the art. *Curr. Opin. Organ Transplant.* **2008**, *13*, 53–58. (c) White, F. A.; Wilson, N. M. Chemokines as pain mediators and modulators. *Curr. Opin. Anaesthesiol.* **2008**, *21*, 580–585. (d) Bhangoo, S. K.; Ren, D.; Miller, R. J.; Chan, D. M.; Ripsch, M. S.; Weiss, C.; McGinnis, C.; White, F. A. CXCR4 chemokine receptor signaling mediates pain hypersensitivity in association with antiretroviral toxic neuropathy. *Brain Behav. Immunol.* **2007**, *21*, 581–591. (e) Savarin-Vuaillat, C.; Ransohoff, R. M. Chemokines and

chemokine receptors in neurological disease: raise, retain, or reduce? *Neurotherapeutics* **2007**, *4*, 590–601. (f) Mines, M.; Ding, Y.; Fan, G. H. The many roles of chemokine receptors in neurodegenerative disorders: emerging new therapeutical strategies. *Curr. Med. Chem.* **2007**, *14*, 2456–2470. (g) Mélik-Parsadaniantz, S.; Rostène, W. Chemokines and neuromodulation. *J. Neuroimmunol.* **2008**, *198*, 62–68.

(7) (a) Aime, S.; Castelli, D. D.; Crich, S. G.; Gianolio, E.; Terreno, E. Pushing the Sensitivity Envelope of Lanthanide-Based Magnetic Resonance Imaging (MRI) Contrast Agents for Molecular Imaging Applications. *Acc. Chem. Res.* **2009**, *42*, 822–831. (b) Shokeen, M.; Anderson, C. J. Molecular Imaging of Cancer with Copper-64 Radiopharmaceuticals and Positron Emission Tomography (PET). *Acc. Chem. Res.* **2009**, *42*, 832–841. (c) De Jong, M.; Breeman, W. A. P.; Kwekkeboom, D. J.; Valkema, R.; Krenning, E. P. Tumor Imaging and Therapy Using Radiolabeled Somatostatin Analogues. *Acc. Chem. Res.* **2009**, *42*, 873–880. (d) Major, J. L.; Meade, T. J. Bioresponsive, Cell-Penetrating, and Multimeric MR Contrast Agents. *Acc. Chem. Res.* **2009**, *42*, 893–903. (e) Tweedle, M. F. Peptide-Targeted Diagnostics and Radiotherapeutics. *Acc. Chem. Res.* **2009**, *42*, 958–968. (f) Schottelius, M.; Laufer, B.; Kessler, H.; Wester, H. J. Ligands for Mapping alpha(v)beta(3)-Integrin Expression in Vivo. *Acc. Chem. Res.* **2009**, *42*, 969–980.

(8) Thumshirn, G.; Hersel, U.; Goodman, S. L.; Kessler, H. Multimeric cyclic RGD peptides as potential tools for tumor targeting: Solid-phase peptide synthesis and chemoselective oxime ligation. *Chem.—Eur. J.* **2003**, *9*, 2717–2725.

(9) (a) Poethko, T.; Schottelius, M.; Thumshirn, G.; Herz, M.; Haubner, R.; Henriksen, G.; Kessler, H.; Schwaiger, M.; Wester, H. J. Chemoselective pre-conjugate radiohalogenation of unprotected mono- and multimeric peptides via oxime formation. *Radiochim. Acta* **2004**, *92*, 317–327. (b) Vagner, J.; Handl, H. L.; Monguchi, Y.; Jana, U.; Begay, L. J.; Mash, E. A.; Hruby, V. J.; Gillies, R. J. Rigid linkers for bioactive peptides. *Bioconjugate Chem.* **2006**, *17*, 1545–1550. (c) Wester, H. J.; Kessler, H. Molecular targeting with peptides or peptide−polymer conjugates: Just a question of size? *J. Nucl. Med.* **2005**, *46*, 1940–1945.

(10) Kessler, H.; Schudok, M.; Haupt, A. In *Peptides*; Jung, G., Bayer, E., Eds.; Walter de Gruyter: Tübingen, Germany, 1988; pp 664−666.

(11) (a) Mammen, M.; Choi, S. K.; Whitesides, G. M. Polyvalent interactions in biological systems: implications for design and use of multivalent ligands and inhibitors. *Angew. Chem. Int. Ed.* **1998**, *37*, 2755–2794. (b) Kiessling, L. L.; Gestwicki, J. E.; Strong, L. E. Synthetic multivalent ligands as probes of signal transduction. *Angew. Chem., Int. Ed. Engl.* **2006**, *45*, 2348–2368.

(12) Crump, M. P.; Gong, J. H.; Loetscher, P.; Rajarathnam, K.; Amara, A.; Arenzana-Seisdedos, F.; Virelizier, J. L.; Baggiolini, M.; Sykes, B. D.; Clark-Lewis, I. Solution structure and basis for functional activity of stromal cell-derived factor-1; dissociation of CXCR4 activation from binding and inhibition of HIV-1. *EMBO J.* **1997**, *16*, 6996–7007.

(13) (a) De Clercq, E.; Yamamoto, N.; Pauwels, R.; Balzarini, J.; Witvrouw, M.; De Vreese, K.; Debyser, Z.; Rosenwirth, B.; Peichl, P.; Datema, R.; et al. Highly potent and selective inhibition of human immunodeficiency virus by the bicyclam derivative JM3100. *Antimicrob. Agents Chemother.* **1994**, *38*, 668–674. (b) De Clercq, E. The AMD3100 story: the path to the discovery of a stem cell mobilizer (Mozobil). *Biochem. Pharmacol.* **2009**, *77*, 1655–1664.

(14) Zhan, W. Q.; Liang, Z. X.; Zhu, A. Z.; Kurtkaya, S.; Shim, H.; Snyder, J. P.; Liotta, D. C. Discovery of small molecule CXCR4 antagonists. *J. Med. Chem.* **2007**, *50*, 5655–5664.

(15) (a) Ojida, A.; Mito-oka, Y.; Inoue, M.; Hamachi, I. First artificial receptors and chemosensors toward phosphorylated peptide in aqueous solution. *J. Am. Chem. Soc.* **2002**, *124*, 6256–6258. (b) Loetscher, P.; Gong, J. H.; Dewald, B.; Baggiolini, M.; Clark-Lewis, I. N-Terminal peptides of stromal cell-derived factor-1 with CXC chemokine receptor 4 agonist and antagonist activities. *J. Biol. Chem.* **1998**, *273*, 22279–22283. (c) Liang, X. CXCR4, inhibitors and mechanisms of action. *Chem. Biol. Drug Des.* **2008**, *72*, 97–110. (d) Heveker, N.; Tissot, M.; Thuret, A.; Schneider-Mergener, J.; Alizon, M.; Roch, M.; Marullo, S. Pharmacological properties of peptides derived from stromal cell-derived factor 1: study on human polymorphonuclear cells. *Mol. Pharmacol.* **2001**, *59*, 1418–1425.

(16) Tamamura, H.; Ojida, A.; Ogawa, T.; Tsutsumi, H.; Masuno, H.; Nakashima, H.; Yamamoto, N.; Hamachi, I.; Fujii, N. Identification of a new class of low molecular weight antagonists against the chemokine receptor CXCR4 having the dipicolylamine−zinc(II) complex structure. *J. Med. Chem.* **2006**, *49*, 3412–3415.

(17) Faber, A.; Roderburg, C.; Wein, F.; Saffrich, R.; Seckinger, A.; Horsch, K.; Diehlmann, A.; Wong, D.; Bridger, G.; Eckstein, V.; Ho, A. D.; Wagner, W. The many facets of SDF-1 alpha, CXCR4 agonists and antagonists on hematopoietic progenitor cells. *J. Biomed. Biotechnol.* **2007**, 10.

(18) (a) Hereld, D.; Jin, T. Slamming the DOR on chemokine receptor signaling: Heterodimerization silences ligand-occupied CXCR4 and delta-opioid receptors. *Eur. J. Immunol.* **2008**, *38*, 334–337. (b) Levoye, A.; Balabanian, K.; Baleux, F.; Bachelerie, F.; Lagane, B. CXCR7 heterodimerizes with CXCR4 and regulates CXCL12-mediated G protein signaling. *Blood* **2009**, *113*, 6085–6093.

(19) Wu, B.; Chien, E. Y.; Mol, C. D.; Fenalti, G.; Liu, W.; Katritch, V.; Abagyan, R.; Brooun, A.; Wells, P.; Bi, F. C.; Hamel, D. J.; Kuhn, P.; Handel, T. M.; Cherezov, V.; Stevens, R. C. Structures of the CXCR4 Chemokine GPCR with Small-Molecule and Cyclic Peptide Antagonists. *Science* **2010**, *330*, 1066–1071.

(20) Kiessling, L. L.; Gestwicki, J. E.; Strong, L. E. Synthetic multivalent ligands in the exploration of cell−surface interactions. *Curr. Opin. Chem. Biol.* **2000**, *4*, 696–703.

(21) Gazit, A.; Osherov, N.; Gilon, C.; Levitzki, A. Tyrphostins. 6. Dimeric benzylidenemalononitrile tyrophostins: potent inhibitors of EGF receptor tyrosine kinase in vitro. *J. Med. Chem.* **1996**, *39*, 4905–4911.

(22) (a) Poethko, T.; Schottelius, M.; Thumshirn, G.; Hersel, U.; Herz, M.; Henriksen, G.; Kessler, H.; Schwaiger, M.; Wester, H. J. Two-step methodology for high-yield routine radiohalogenation of peptides: F-18-labeled RGD and octreotide analogs. *J. Nucl. Med.* **2004**, *45*, 892–902. (b) Li, Z. B.; Chen, K.; Chen, X. ^{68}Ga-labeled multimeric RGD peptides for microPET imaging of integrin alpha(v)beta(3) expression. *Eur. J. Nucl. Med. Mol. Imaging* **2008**, *35*, 1100–1108.

(23) (a) Miyata, T.; Tokunaga, F.; Yoneya, T.; Yoshikawa, K.; Iwanaga, S.; Niwa, M.; Takao, T.; Shimonishi, Y. Antimicrobial peptides, isolated from horseshoe crab hemocytes, tachyplesin II, and polyphemusins I and II: chemical structures and biological activity. *J. Biochem. (Tokyo)* **1989**, *106*, 663–668. (b) Tamamura, H.; Xu, Y. O.; Hattori, T.; Zhang, X. Y.; Arakaki, R.; Kanbara, K.; Omagari, A.; Otaka, A.; Ibuka, T.; Yamamoto, N.; Nakashima, H.; Fujii, N. A low-molecular-weight inhibitor against the chemokine receptor CXCR4: A strong anti-HIV peptide T140. *Biochem. Biophys. Res. Commun.* **1998**, *253*, 877–882.

(24) (a) Masuda, M.; Nakashima, H.; Ueda, T.; Naba, H.; Ikoma, R.; Otaka, A.; Terakawa, Y.; Tamamura, H.; Ibuka, T.; Murakami, T.; Koyanagi, Y.; Waki, M.; Matsumoto, A.; Yamamoto, N.; Funakoshi, S.; Fujii, N. A Novel Anti-HIV Synthetic Peptide, T-22 ([Tyr^{5,12},Lys^{7}]-Polyphemusin-II). *Biochem. Biophys. Res. Commun.* **1992**, *189*, 845–850. (b) Tamamura, H.; Waki, M.; Imai, M.; Otaka, A.; Ibuka, T.; Waki, K.; Miyamoto, K.; Matsumoto, A.; Murakami, T.; Nakashima, H.; Yamamoto, N.; Fujii, N. Downsizing of an HIV-cell fusion inhibitor, T22 ([Tyr(5,12), Lys(7)]-polyphemusin II), with the maintenance of anti-HIV activity and solution structure. *Bioorg. Med. Chem.* **1998**, *6*, 473–479. (c) Tamamura, H.; Arakaki, R.; Funakoshi, H.; Imai, M.; Otaka, A.; Ibuka, T.; Nakashima, H.; Murakami, T.; Waki, M.; Matsumoto, A.; Yamamoto, N.; Fujii, N. Effective lowly cytotoxic analogs of an HIV-cell fusion inhibitor, T22 ([Tyr^{5,12},Lys^{7}]-polyphemusin II). *Bioorg. Med. Chem.* **1998**, *6*, 231–238. (d) Tamamura, H.; Omagari, A.; Oishi, S.; Kanamoto, T.; Yamamoto, N.; Peiper, S. C.; Nakashima, H.; Otaka, A.; Fujii, N. Pharmacophore identification of a specific CXCR4 inhibitor, T140, leads to development of effective anti-HIV agents with very high selectivity indexes. *Bioorg. Med. Chem. Lett.* **2000**, *10*, 2633–2637.

(25) Fujii, N.; Oishi, S.; Hiramatsu, K.; Araki, T.; Ueda, S.; Tamamura, H.; Otaka, A.; Kusano, S.; Terakubo, S.; Nakashima, H.; Broach, J. A.; Trent, J. O.; Wang, Z. X.; Peiper, S. C. Molecular-size reduction of a potent CXCR4-chemokine antagonist using orthogonal combination of conformation- and sequence-based libraries. *Angew. Chem. Int. Ed.* **2003**, *42*, 3251–3253.

(26) Haubner, R.; Kuhnast, B.; Mang, C.; Weber, W. A.; Kessler, H.; Wester, H. J.; Schwaiger, M. [F-18]Galacto-RGD: Synthesis, radiolabeling, metabolic stability, and radiation dose estimates. *Bioconjugate Chem.* **2004**, *15*, 61–69.

(27) (a) Zhang, W. B.; Navenot, J. M.; Haribabu, B.; Tamamura, H.; Hiramatu, K.; Omagari, A.; Pei, G.; Manfredi, J. P.; Fujii, N.; Broach, J. R.; Peiper, S. C. A point mutation that confers constitutive activity to CXCR4 reveals that T140 is an inverse agonist and that AMD3100 and ALX40−4C axe weak partial agonists. *J. Biol. Chem.* **2002**, *277*, 24515–24521. (b) Trent, J. O.; Wang, Z. X.; Murray, J. L.; Shao, W.; Tamamura, H.; Fujii, N.; Peiper, S. C. Lipid bilayer simulations of CXCR4 with inverse agonists and weak partial agonists. *J. Biol. Chem.* **2003**, *278*, 47136–47144. (c) Wang, Z.-x.; Tamamura, H.; Frilot, N.; Broach, J.; Fujii, N.; Peiper, S. Screening and characterization of cyclic pentapeptide CXCR4 antagonists/inverse agonists using a pheromone responsive reporter gene in *Saccharomyces cerevisiae*: Utility of G protein coupled receptor constitutively active mutants. In *Chemokine Biology—Basic Research and Clinical Application*; Neote, K. L., Gordon, L., Moser, B., Eds.; Birkhäuser: Basel, 2007; pp 61−77.

(28) Tanaka, T.; Nomura, W.; Narumi, T.; Masuda, A.; Tamamura, H. Bivalent Ligands of CXCR4 with Rigid Linkers for Elucidation of the Dimerization State in Cells. *J. Am. Chem. Soc.* **2010**, *132*, 15899–901.

(29) Ueda, S.; Oishi, S.; Wang, Z. X.; Araki, T.; Tamamura, H.; Cluzeau, J.; Ohno, H.; Kusano, S.; Nakashima, H.; Trent, J. O.; Peiper, S. C.; Fujii, N. Structure−activity relationships of cyclic peptide-based chemokine receptor CXCR4 antagonists: disclosing the importance of side-chain and backbone functionalities. *J. Med. Chem.* **2007**, *50*, 192–198.

(30) Demmer, O.; Koglin, N.; Kessler, H.; Wester, H. J. Cyclic peptides for targeting CXCR4 chemokine receptor expression. *J. Pept. Sci.* **2006**, *12*, 172–172.

(31) Demmer, O.; Gourni, E.; Schumacher, U.; Wester, H. J.; Kessler, H. PET imaging of CXCR4 receptors in cancer by a new optimized ligand. *ChemMedChem*, **2011**, DOI 10.1002/cmdc.201100320

(32) Demmer, O.; Dijkgraaf, I.; Schottelius, M.; Wester, H. J.; Kessler, H. Introduction of functional groups into peptides via *N*-alkylation. *Org. Lett.* **2008**, *10*, 2015–2018.

(33) (a) Demmer, O.; Frank, A. O.; Kessler, H. Design of Cyclic Peptides. In *Design of Peptides and Proteins for Biopharmaceutical Applications: Applications for Therapeutic Agents and Biomedical Research*; Jensen, K. J., Ed.; Wiley: New York, 2009; pp 133−176. (b) Kessler, H.; Kutscher, B. Peptide Conformations 0.40. Cyclic Hexapeptide Analogs of Thymopoietin—Synthesis and Conformational Analysis. *Liebigs Ann. Chem.* **1986**, 914–931.(c) Gilon, C.; Mang, C.; Lohof, E.; Friedler, A.; Kessler, H. Synthesis of Peptides and Peptidomimetics. In *Houben-Weyl: Methods of Organic Chemistry*; Goodman, M., Felix, L., Moroder, L., Toniolo, C., Eds.; Thieme Verlag: Stuttgart, 2003; pp 461−542.

(34) Biron, E.; Chatterjee, J.; Kessler, H. Optimized selective *N*-methylation of peptides on solid support. *J. Pept. Sci.* **2006**, *12*, 213–219.

(35) Müller, A.; Vogt, C.; Sewald, N. Synthesis of Fmoc-beta-homoamino acids by ultrasound-promoted Wolff rearrangement. *Synthesis (Stuttgart)* **1998**, 837–841.

(36) (a) Moepps, B.; Frodl, R.; Rodewald, H. R.; Baggiolini, M.; Gierschik, P. Two murine homologues of the human chemokine receptor CXCR4 mediating stromal cell-derived factor 1 alpha activation of G(12) are differentially expressed in vivo. *Eur. J. Immunol.* **1997**, *27*, 2102–2112. (b) Hanaoka, H.; Mukai, T.; Tamamura, H.; Mori, T.; Ishino, S.; Ogawa, K.; Iida, Y.; Doi, R.; Fujii, N.; Saji, H. Development of a In-111-labeled peptide derivative targeting a chemokine receptor, CXCR4, for imaging tumors. *Nucl. Med. Biol.* **2006**, *33*, 489–494. (c) Jacobson, O.; Weiss, I. D.; Szajek, L.; Farber, J. M.; Kiesewetter, D. O. Cu-64-AMD3100—a novel imaging agent for targeting chemokine receptor CXCR4. *Bioorg. Med. Chem.* **2009**, *17*, 1486–1493. (d) Nimmagadda, S.; Pullambhatla, M.; Stone, K.; Green, G.; Bhujwalla, Z. M.; Pomper, M. G. Molecular Imaging of CXCR4 Receptor Expression in Human Cancer Xenografts with [Cu-64]AMD3100 Positron Emission Tomography. *Cancer Res.* **2010**, *70*, 3935–3944.

(37) (a) Ichiyama, K.; Yokoyama-Kumakura, S.; Tanaka, Y.; Tanaka, R.; Hirose, K.; Bannai, K.; Edamatsu, T.; Yanaka, M.; Niitani, Y.; Miyano-Kurosaki, N.; Takaku, H.; Koyanagi, Y.; Yamamoto, N. A duodenally absorbable CXC chemokine receptor 4 antagonist, KRH-1636, exhibits a potent and selective anti-HIV-1 activity. *Proc. Natl. Acad. Sci. U.S.A.* **2003**, *100*, 4185–4190. (b) Fujii, N.; Nakashima, H.; Tamamura, H. The therapeutic potential of CXCR4 antagonists in the treatment of HIV. *Expert Opin. Invest. Drug* **2003**, *12*, 185–195.

(38) Friesner, R. A.; Murphy, R. B.; Repasky, M. P.; Frye, L. L.; Greenwood, J. R.; Halgren, T. A.; Sanschagrin, P. C.; Mainz, D. T. Extra precision Glide: Docking and scoring incorporating a model of hydrophobic enclosure for protein-ligand complexes. *J. Med. Chem.* **2006**, *49*, 6177–6196.

(39) (a) Clark-Lewis, I.; Kim, K. S.; Rajarathnam, K.; Gong, J. H.; Dewald, B.; Moser, B.; Baggiolini, M.; Sykes, B. D. Structure−activity relationships of chemokines. *J. Leukocyte Biol.* **1995**, *57*, 703–11. (b) Wells, T. N.; Power, C. A.; Lusti-Narasimhan, M.; Hoogewerf, A. J.; Cooke, R. M.; Chung, C. W.; Peitsch, M. C.; Proudfoot, A. E. Selectivity and antagonism of chemokine receptors. *J. Leukocyte Biol.* **1996**, *59*, 53–60. (c) Gupta, S. K.; Pillarisetti, K.; Thomas, R. A.; Aiyar, N. Pharmacological evidence for complex and multiple site interaction of CXCR4 with SDF-1alpha: implications for development of selective CXCR4 antagonists. *Immunol. Lett.* **2001**, *78*, 29–34.

(40) (a) Gerlach, L. O.; Jakobsen, J. S.; Jensen, K. P.; Rosenkilde, M. R.; Skerlj, R. T.; Ryde, U.; Bridger, G. J.; Schwartz, T. W. Metal ion enhanced binding of AMD3100 to Asp^{262} in the CXCR4 receptor. *Biochemistry* **2003**, *42*, 710–717. (b) Khan, A.; Silversides, J. D.; Madden, L.; Greenman, J.; Archibald, S. J. Fluorescent CXCR4 chemokine receptor antagonists: metal activated binding. *Chem. Commun. (Cambridge, UK)* **2007**, 416–418. (c) Khan, A.; Nicholson, G.; Greenman, J.; Madden, L.; McRobbie, G.; Pannecouque, C.; De Clercq, E.; Ullom, R.; Maples, D. L.; Maples, R. D.; Silversides, J. D.; Hubin, T. J.; Archibald, S. J. Binding Optimization through Coordination Chemistry: CXCR4 Chemokine Receptor Antagonists from Ultrarigid Metal Complexes. *J. Am. Chem. Soc.* **2009**, *131*, 3416–3417. (d) Heppeler, A.; Froidevaux, S.; Mäcke, H. R.; Jermann, E.; Béhé, M.; Powell, P.; Hennig, M. Radiometal-Labelled Macrocyclic Chelator-Derivatised Somatostatin Analogue with Superb Tumour-Targeting Properties and Potential for Receptor-Mediated Internal Radiotherapy. *Chem. Eur. J.* **1999**, *5*, 1974–1981. (e) Liu, S.; He, Z.; Hsieh, W.-Y.; Fanwick, P. E. Synthesis, Characterization, and X-ray Crystal Structure of In(DOTA-AA) (AA = p-Aminoanilide): A Model for ^{111}In-Labeled DOTA-Biomolecule Conjugates. *Inorg. Chem.* **2003**, *42*, 8831–8837.

(41) Reubi, J. C.; Schar, J. C.; Waser, B.; Wenger, S.; Heppeler, A.; Schmitt, J. S.; Mäcke, H. R. Affinity profiles for human somatostatin receptor subtypes SST1-SST5 of somatostatin radiotracers selected for scintigraphic and radiotherapeutic use. *Eur. J. Nucl. Med.* **2000**, *27*, 273–282.

(42) Hamzé, A.; Hernandez, J. F.; Martinez, J. Synthesis of (*R*) and (*S*) enantiomers of Fmoc-protected 1,2,4-oxadiazole-containing $beta^3$-amino acids from Fmoc-(*R*)-beta-HAsp(OtBu)-OH. *Tetrahedron Lett.* **2003**, *44*, 6079–6082.

(43) Herzner, H.; Kunz, H. Spacer-separated sialyl LewisX cyclopeptide conjugates as potential E-selectin ligands. *Carbohydr. Res.* **2007**, *342*, 541–557.

(44) Castonguay, R.; Lherbet, C.; Keillor, J. W. Mapping of the active site of rat kidney gamma-glutamyl transpeptidase using activated esters and their amide derivatives. *Bioorg. Med. Chem.* **2002**, *10*, 4185–4191.

(45) Mizukami, S.; Takikawa, R.; Sugihara, F.; Hori, Y.; Tochio, H.; Walchli, M.; Shirakawa, M.; Kikuchi, K. Paramagnetic relaxation-based F-19 MRI probe to detect protease activity. *J. Am. Chem. Soc.* **2008**, *130*, 794–795.

(46) Wishart, D. S.; Bigam, C. G.; Yao, J.; Abildgaard, F.; Dyson, H. J.; Oldfield, E.; Markley, J. L.; Sykes, B. D. 1H, 13C and 15N chemical shift referencing in biomolecular NMR. *J. Biomol. NMR* **1995**, *6*, 135–140.

(47) Piotto, M.; Saudek, V.; Sklenar, V. Gradient-tailored excitation for single-quantum NMR spectroscopy of aqueous solutions. *J. Biomol. NMR* **1992**, *2*, 661–665.

(48) (a) Kessler, H.; Seip, S. NMR of Peptides. In *Two-Dimensional NMR-Spectroscopy, Applications for Chemists and Biochemists*; Croasmun,

W. R., Carlson, M. K., Eds.; VCH: New York, 1994; pp 619−654. (b) Kessler, H.; Schmitt, W. Peptides and Polypeptides. In *Encyclopedia of Nuclear Magnetic Resonance*; Grant, D. M., Harris, R. K., Eds.; J. Wiley & Sons: New York, 1996; pp 3527−3537.

(49) (a) Bax, A.; Summers, M. F. H-1 and C-13 Assignments from Sensitivity-Enhanced Detection of Heteronuclear Multiple-Bond Connectivity by 2d Multiple Quantum Nmr. *J. Am. Chem. Soc.* **1986**, *108*, 2093–2094. (b) Bermel, W.; Wagner, K.; Griesinger, C. Proton-Detected C,H Correlation Via Long-Range Couplings with Soft Pulses—Determination of Coupling-Constants. *J. Magn. Reson.* **1989**, *83*, 223–232. (c) Kessler, H.; Schmieder, P.; Kock, M.; Kurz, M. Improved Resolution in Proton-Detected Heteronuclear Long-Range Correlation. *J. Magn. Reson.* **1990**, *88*, 615–618.

(50) Griesinger, C.; Sorensen, O. W.; Ernst, R. R. Practical Aspects of the E-Cosy Technique—Measurement of Scalar Spin Spin Coupling Constants in Peptides. *J. Magn. Reson.* **1987**, *75*, 474–492.

(51) (a) Bothner-By, A. A.; Stephens, R. L.; Lee, J. M.; Warren, C. D.; Jeanloz, R. W. Structure Determination of a Tetrasaccharide—Transient Nuclear Overhauser Effects in the Rotating Frame. *J. Am. Chem. Soc.* **1984**, *106*, 811–813. (b) Kessler, H.; Griesinger, C.; Kerssebaum, R.; Wagner, K.; Ernst, R. R. Separation of Cross-Relaxation and J-Cross-Peaks in 2D Rotating-Frame NMR Spectroscopy. *J. Am. Chem. Soc.* **1987**, *109*, 607–609.

(52) (a) Berendsen, H. J. C.; van der Spoel, D.; van Drunen, R. GROMACS: A message-passing parallel molecular dynamics implementation. *Comput. Phys. Commun.* **1995**, *91*, 43–56. (b) Lindahl, E.; Hess, B.; van der Spoel, D. GROMACS 3.0: A package for molecular simulation and trajectory analysis. *J. Mol. Model.* **2001**, *7*, 306–317.

(53) Berendsen, H. J. C.; Postma, J. P. M.; van Gunsteren, W. F.; Dinola, A.; Haak, J. R. Molecular Dynamics with Coupling to an External Bath. *J. Chem. Phys.* **1984**, *81*, 3684–3690.

(54) Schrödinger Suite 2009 Protein Preparation Wizard, Epik version 2.0; Impact version 5.5; Prime version 2.1; Schrödinger, LLC: New York, NY, 2009.

(55) Friesner, R. A.; Murphy, R. B.; Repasky, M. P.; Frye, L. L.; Greenwood, J. R.; Halgren, T. A.; Sanschagrin, P. C.; Mainz, D. T. Extra precision glide: docking and scoring incorporating a model of hydrophobic enclosure for protein-ligand complexes. *J. Med. Chem.* **2006**, *49*, 6177–6196.

(56) Pettersen, E. F.; Goddard, T. D.; Huang, C. C.; Couch, G. S.; Greenblatt, D. M.; Meng, E. C.; Ferrin, T. E. UCSF Chimera—a visualization system for exploratory research and analysis. *J. Comput. Chem.* **2004**, *25*, 1605–12.